

Research papers

Melting dynamics and energy efficiency of nano-enhanced phase change material (NePCM) with graphene, Al₂O₃, and CuO for superior thermal energy storage (TES)



Anjan Nandi , Nirmalendu Biswas *

^a Department of Power Engineering, Jadavpur University, Salt Lake, Kolkata 700106, India

ARTICLE INFO

Keywords:

Energy storage
Phase change material (PCM)
Nanoparticles
Enhancement
Heat transfer

ABSTRACT

Nano-enhanced phase change materials (NePCMs) have emerged as a promising option for boosting the efficiency of thermal energy storage (TES) systems. This study investigates, through numerical simulations, how the incorporation of nanoparticles such as Al₂O₃, CuO, and Graphene (with concentrations $\varphi = 0.5\% \text{ to } 5\%$) into paraffin wax affects melting performance. The study further examines how key material properties like thermal conductivity, viscosity, and density influence the overall thermal behavior. Also, the effects of varying cavity inclination angles ($\theta = 0^\circ \text{ to } 60^\circ$) and heated wall temperatures ($\Theta = 323 \text{ K to } 343 \text{ K}$) are analyzed. The computational analysis is carried out using computational fluid dynamics (CFD) and the finite volume method to solve the heat transfer equations. Results indicate that although increased nanoparticle concentrations result in higher viscosity, the improvement in thermal conductivity and the reduction in latent heat outweigh the drawbacks, leading to higher energy storage efficiency. Energy efficiency increases by 4.975 % with the addition of 0.5 % Al₂O₃, while Graphene nanoparticles at a 3 % concentration leads to a 7.118 % improvement. The study also shows that increasing the inclination of the cavity angle enhances the melting rate by 43.841 % for pure phase change material (PCM) and 44.865 % for NePCM compared to the horizontal position ($\theta = 0^\circ$). These results demonstrate the potential of NePCMs for improving TES systems and suggest the need for further research to refine NePCM formulations for practical applications in sustainable energy technologies.

1. Introduction

The focus on alternative energy sources has been growing steadily, fueled by an increase in global energy demand due to industrial digitization, fluctuating crude oil prices, rising fossil fuel costs, and increasing concerns over environmental degradation, carbon emissions, and global warming. As of now, no single renewable energy technology can independently supply sufficient energy, necessitating the development of efficient energy storage systems to convert renewable energy into usable forms. In this regard, Thermal Energy Storage (TES) technologies have become essential, particularly for renewable energy systems like solar power, where energy supply is inconsistent. TES essentially stores thermal energy for later use, allowing for better energy management in renewable systems. There are three main types of TES systems: (a) sensible heat storage, which relies on changing the temperature of the storage material; (b) latent heat storage, which takes advantage of phase changes, such as from liquid to solid; and (c)

thermochemical storage, which uses reversible chemical reactions for energy storage. Latent Thermal Energy Storage (LTES) systems, which utilize Phase Change Materials (PCMs), are especially promising due to two significant advantages: their high volumetric energy storage density and their ability to maintain near-isothermal conditions during phase changes. PCMs have melting and freezing points ranging from 288 K to 363 K, making them versatile for various energy storage applications [1]. For optimal TES system performance, a PCM should exhibit several key characteristics, including a melting point within the desired temperature range, consistent thermophysical properties during repeated cycles, minimal supercooling, high specific heat capacity, high latent heat of fusion, and excellent thermal conductivity in both liquid and solid states. Maintaining consistent thermophysical properties during melting and solidification cycles is crucial for developing efficient latent heat storage systems [2,3].

One of the significant challenges of using PCMs in TES systems is their typically low thermal conductivity, which limits system response times during the melting and solidification processes. This limitation

* Corresponding author.

E-mail address: biswas.nirmalendu@gmail.com (N. Biswas).

| Nomenclature | |
|----------------------|---|
| A_{mush} | mushy zone constant ($\text{kg} \cdot \text{m}^{-3} \text{s}^{-1}$) |
| C_p | specific heat ($\text{J} \cdot \text{kg}^{-1} \text{K}^{-1}$) |
| f | liquid fraction |
| g | acceleration due to gravity ($\text{m} \cdot \text{s}^{-2}$) |
| H | height of the cavity (m) |
| k | permeability (m^2) |
| K | thermal conductivity ($\text{W} \cdot \text{m}^{-1} \text{K}^{-1}$) |
| L | latent heat of fusion ($\text{kJ} \cdot \text{kg}^{-1}$) |
| t | Time (s) |
| T | temperature (K) |
| u, v | x and y velocity components (m s^{-1}) |
| W | length of the cavity (m) |
| x, y | Cartesian coordinates (m) |
| <i>Greek symbols</i> | |
| β | thermal expansion coefficient (K^{-1}) |
| Δh | total enthalpy ($\text{kJ} \cdot \text{kg}^{-1}$) |
| δ | constant |
| θ | inclination angle ($^\circ$) |
| Θ | hot wall temperature range (K) |
| μ | fluid dynamic viscosity, ($\text{Nm} \cdot \text{s}^{-2}$) |
| ν | kinetic viscosity ($\text{kg} \cdot \text{m}^{-1} \text{s}^{-1}$) |
| ρ | density ($\text{kg} \cdot \text{m}^{-3}$) |
| ϕ | nanoparticle volume fraction |
| ψ | dimensionless stream function |
| <i>Subscripts</i> | |
| h | hot |
| eff | effective |
| m | melting |
| ref | reference |
| s | solidification |

poses a significant barrier to the large-scale implementation of Latent Heat Storage Systems (LHS) [4]. Researchers have proposed several solutions to overcome this issue, such as modifying the design of PCM containers by adding fins [5–7], heat pipes [8], and metallic foam [9]. A more modern approach to enhancing thermal conductivity involves introducing nanoparticles with high thermal conductivity into PCMs. Due to their small size (ranging from 1 to 100 nm), these nanoparticles offer a high surface area-to-volume ratio, which improves thermal conductivity and accelerates the phase change process. Aluminum oxide (Al_2O_3) [10,11], copper (Cu) [12], copper oxide (CuO) [13,14], graphene [15,16], graphene oxide (GO) [17], gold (Au) [18], silver (Ag) [18–20], silicon carbide (SiC) [21,22], titanium oxide (TiO_2) [23,24], zinc oxide (ZnO) [25,26], carbon nanotubes (single and multiwall) (SCNTs and MWCNTs) [27–29], are the most frequently used nanoparticles for thermal applications.

Recently, there has been interest in improving thermal conductivity in PCM for applications reliant on energy storage. Abdelrahman et al. [10] experimentally investigated the use of Al_2O_3 nanoparticles in concentrations ranging from 0.11 % to 0.77 % with RT35HC as the base PCM to enhance solar cell performance. A cylindrical fin was used as both a heat sink and a thermal conductivity booster. Their results demonstrated that adding cylindrical fins to RT35HC led to a 20 % to 46.3 % reduction in front surface temperature under heat flux conditions ranging from 279 W/m^2 to 820 W/m^2 . The incorporation of Al_2O_3 nanoparticles further amplified this temperature reduction, achieving an overall decrease of up to 52.3 %. Similarly, Ho and Gao [11] used Al_2O_3 nanoparticles mixed with n-octadecane as a base PCM within a vertical square enclosure. The findings showed that increasing the mass fraction of nanoparticles reduced the natural convection heat transfer within the melted region. While this suggests improved thermal conductivity, the increased nanoparticle concentration can hinder convective heat transfer in certain applications. Jourabian et al. [12] conducted a numerical study on the melting process of copper-water nanofluid PCM to improve the efficiency of heat transfer during phase change. Their results highlighted that the volume fraction of nanoparticles plays a crucial role in enhancing heat conduction in the melt zone, leading to quicker melting.

Sharma et al. [13] studied passive cooling for building-integrated photovoltaics using Rubitherm (RT42) as the PCM, combined with copper oxide (CuO) nanoparticles and microfins. Their results showed that microfins alone reduced the temperature of the system by 10.7°C , while the addition of nano-enhanced PCM (NePCM) further reduced it by 12.5°C . Jesumathy et al. [14], working with CuO in paraffin wax, demonstrated that increasing CuO concentrations significantly

improved both natural convection and heat conduction. In another study, Zou et al. [15] examined thermal management for lithium-ion batteries using MWCNT, graphene, and MWCNT/graphene composite PCMs. They found that a 3:7 mass ratio of MWCNT to graphene increased thermal conductivity by up to 124 %, reducing temperatures by 50–63 % compared to pure PCM, which highlights the effectiveness of these composites for battery cooling. Khan and Khan [16] evaluated latent heat storage (LHS) systems using paraffin and Graphene nanoplatelets (GNP). The optimal configuration combined wire-wound fins with 1 % GNP, which improved heat flux and charging time, though higher GNP concentrations led to decreased performance. Safaei et al. [17] investigated solar-driven water desalination using Graphene oxide (GO) mixed with paraffin. Their results showed a 25 % increase in productivity and reduced melting temperatures, particularly at higher wall temperatures. Xu et al. [18] used molecular dynamics simulations to study the impact of gold nanoparticles embedded in PCM microcapsules. The findings revealed that higher heat flux and magnetic fields enhanced thermal conductivity but also increased viscosity, presenting potential limitations in practical applications.

Pradeep et al. [19] examined the use of silver nanoparticles (Ag) in paraffin wax to boost its thermal energy storage capacity. Two concentrations of Ag (0.05 % and 0.1 %) nanoparticles were tested, and the results showed that both the melting and solidification temperatures were reduced. Moreover, higher concentrations of Ag nanoparticles improved the energy storage capacity of the material, suggesting potential applications in solar energy systems. The study of Zeng et al. [20] introduced organic PCM composites containing silver nanoparticles (Ag) and found that these composites exhibited improved thermal conductivity while maintaining substantial phase-change enthalpy. Although the phase-change temperature was slightly lower than that of pure PCM, the composite materials demonstrated promising thermal stability and uniform dispersion of Ag nanoparticles, making them suitable for practical TES applications.

Maher et al. [21] address the need for improved thermal conductivity in PCMs like paraffin wax. By incorporating silicon carbide (SiC) and silver (Ag) nanoparticles, significant enhancements were achieved. For instance, a 15 % wt. SiC composite showed a 58.2 % increase in thermal conductivity, while a 15 % wt. Ag composite exhibited a 31.2 % improvement. However, higher nanoparticle concentrations (>5 % wt.) led to slight reductions in latent heat of fusion, melting point, and specific heat capacity. These findings are crucial for designing efficient nano-PCM-based thermal energy storage systems. The study of Al-Waeli et al. [22] explores enhancing photovoltaic/thermal (PV/T) system efficiency by adding nanomaterials to the cooling fluid. Three

nanomaterials (Al_2O_3 , CuO , and SiC) were tested in water at different volume fractions ($\varphi = 0.5\text{--}4\%$). Results showed nanofluids significantly boosted thermal conductivity with minimal impact on fluid properties. Silicon carbide (SiC) nanoparticles demonstrated superior stability and thermal conductivity compared to others. Despite the higher conductivity of copper oxide than aluminum oxide, it showed lower stability, though still relatively stable. So the nanofluids effectively lowered indoor PV/T system temperature and improved power generation. Babapoor et al. [22] explored how various nanoparticles such as Al_2O_3 , CuO , TiO_2 , and Graphene are affected the thermophysical properties of paraffin during solidification. Their results revealed that graphene provided the most significant improvement in thermal conductivity, especially at concentrations of 3 % wt.

These findings of Bae et al. [24] are vital for thermal management in various systems, especially during solidification. This study examines the dispersion stability of rutile TiO_2 powder synthesized via a unique process (HPPLT). Various electrolytes were added to both aqueous and organic media. Zeta potential measurements showed a charge reversal from negative to positive on TiO_2 particle surfaces with electrolyte addition. Notably, electrostatic repulsion between dispersed TiO_2 particles was stronger in organic media than in aqueous media, influenced by solvent properties like viscosity and dielectric constant. Surface potentials of TiO_2 particles were influenced by particle properties, pH, dispersion medium, and ionic species valence, governing their colloidal behavior.

Harikrishnan et al. [25] explore new composite PCMs for building heating. The composites, consisting of a 70:30 mixture of lauric acid (LA) and stearic acid (SA) as base materials, incorporate TiO_2 , ZnO , and CuO nanoparticles at 1.0 % wt. Sodium dodecylbenzene sulfonate (SDBS) ensures stability. SEM analyzes nanoparticle morphology, while DSC and TGA assess phase change temperatures, latent heat, and thermal stability. Thermal conductivity increases significantly, with CuO nanoparticles showing the highest enhancement. Composite PCMs with CuO nanoparticles demonstrate greater time savings in melting and solidification processes compared to TiO_2 and ZnO nanoparticles and the base material, making them promising for building heating applications. The study explores nanocomposite-NePCMs by mixing paraffin with alumina (Al_2O_3), titania (TiO_2), silica (SiO_2), and zinc oxide (ZnO) at concentrations of 1.0, 2.0, and 3.0 % wt. done by Teng et al. [26] TiO_2 demonstrates superior performance in enhancing heat conduction and thermal storage, lowering melting onset temperature and increasing solidification onset temperature. It enables a wider temperature range for phase-change heat application, with only a 0.46 % decrease in phase-change heat compared to pure paraffin. This study highlights the potential of TiO_2 for improving thermal storage characteristics in NePCMs.

Wang et al. [27] tackled the issue of dispersing multi-walled carbon nanotubes (CNTs) in an organic matrix by using a mechano-chemical process that added hydroxide radicals to the CNT surfaces. This treatment allowed stable dispersion in palmitic acid without the need for surfactants and resulted in a significant increase in thermal conductivity—approximately 30 % higher than that of acid-treated CNTs. Bahiraei et al. [28] studied the use of carbon-based nanoparticles to improve thermal conductivity in PCMs used in devices such as electric vehicle batteries. While these nanoparticles increased solid-phase conductivity by up to 1100 %, they also raised dynamic viscosity, reducing natural convection and hindering heat transfer in melted PCMs. Zabalegui et al. [29] examined nanofluids with paraffin, finding that smaller CNTs reduced the latent heat of fusion, possibly due to mechanisms like interfacial liquid layering and Brownian motion. However, they concluded that nanofluids may not notably enhance TES efficiency, as performance varies with particle size and material characteristics. These studies underscore the trade-off between improving thermal conductivity and the negative impacts on viscosity and convection, affecting TES systems.

Abdulmunem et al. [30] examined the melting behavior of PCM in a rectangular container under various tilt angles (0°, 30°, 60°, and 90°)

using both experimental and numerical methods. They found that lower tilt angles hinder the melting process due to decreased convection, concluding that higher tilt angles improve PCM performance. Wang et al. [31] conducted a numerical study focusing on the melting of paraffin within a rectangular cavity across a range of inclination angles from 0° to 180°. Their analysis showed that as the angle increased, the melting time extended non-linearly, suggesting that natural convection significantly influenced both the temperature distribution and the solid-liquid interface.

Xie and Wu [32] investigated PCM melting in a 2D square cavity with varying aspect ratios (AR) under a constant heat flux. Their results indicated that bottom-wall heating accelerated the melting process, particularly for AR values >1, while an increase in AR led to longer melting times due to natural convection patterns, such as Rayleigh-Benard cells. Hekmat et al. [33] explored how PCM container geometry and nanoparticle concentrations (0 %, 0.02 %, and 0.04 %) affected melting and solidification rates. Their findings showed that the combination of fins and nanoparticles provided maximum enhancements of 80 % in melting and 66 % in solidification, with different container shapes showing varying improvements. Kamkari and Amlashi [34] analyzed the melting of PCM in inclined enclosures (0° and 45°), demonstrating that natural convection accelerated melting by 52 % and 37 %, respectively, compared to vertical configurations. Their simulations deviated by <6.5 % from experimental results and provided new correlations for liquid fraction, energy storage, and Nusselt number.

In recent years, there has been growing interest in advancing thermal energy storage technologies to facilitate the transition towards cleaner and more sustainable energy systems. PCMs have emerged as a promising solution for efficient energy storage and utilization due to their ability to store and release latent heat during phase transitions. However, traditional PCM systems often exhibit limitations in terms of heat transfer rates and overall performance. To address these challenges and enhance the thermal properties of PCM systems, researchers have turned to the integration of nanoparticles to create NePCMs. By dispersing nanoparticles within the PCM matrix, significant improvements in thermal conductivity, heat transfer rates, and energy storage capacity can be achieved. This innovation holds great potential for various cleaner energy applications, including solar thermal energy storage, waste heat recovery, and thermal management in electronics and buildings. While the performance of NePCMs has been extensively studied under conventional conditions, there remains a gap in understanding their behavior under inclined orientations, such as those encountered in solar thermal collectors and building integrated systems. The inclination angle of the collector or storage system can significantly influence the distribution of solar radiation, heat transfer mechanisms, and overall energy storage efficiency. Therefore, investigating the impact of the angle of inclination on thermal efficiency in NePCMs is crucial for optimizing their utilization in cleaner energy applications.

The objective of the present investigation is to assess the thermal performance and energy storage capabilities of NePCM-based thermal systems under various operating conditions. Specifically, the investigation aims for:

- Assess the impact of nano-additives on the thermal characteristics and performance of PCM-based energy storage systems.
- Investigate the impact of different volume fractions and types of nanoparticles on the melting/charging processes and energy storage efficiency.
- Investigate how the varying cavity inclination angles impact the thermal performance and energy storage capabilities of NePCM-based thermal systems. Analyze how changes in the orientation of energy storage systems affect the heat transfer rate, phase change dynamics, and total system efficiency.
- Investigate the impact of heated wall temperature on the melting processes, melting speed, energy storage rate, and overall efficiency.

- e) Analyze the effectiveness of NePCM systems in enhancing energy storage capacity, thermal conductivity, and overall thermal performance compared to traditional PCM-based systems.
- f) Optimize the design parameters, such as volume fraction (φ), nanoparticle type, and inclination angles (θ) for NePCM-based energy storage systems to maximize energy efficiency and melting performance. Determine the ideal orientation that enhances the heat transfer effectiveness, to maximize energy storage efficiency and thermal stability, and promotes sustainable energy utilization.

The investigation aims to advance understanding of the role of cavity inclination on the NePCM-based energy storage systems and their potential for enhancing energy efficiency and sustainability in cleaner energy applications. Through numerical simulation and analysis, the study seeks to provide valuable insights and guidance for the design and deployment of NePCM systems in real-world scenarios thereby fostering sustainable and efficient energy storage solutions for a greener future. Thus, this study investigates the influence of different nanoparticles namely, Al_2O_3 , CuO , and Graphene with varying volume fractions from $\varphi = 0.5$ to 5 % on melting rates and total melting times. Further investigation has been done on the effect of inclination angles from $\theta = 0^\circ$ to 60° on the thermal behavior of the best type of nanoparticle with optimum volume fraction. For real-world thermal storage systems, particularly in solar energy applications or building-integrated thermal systems, optimizing the angle of the storage unit could significantly enhance system efficiency. Systems designed with adjustable angles might offer flexibility in maximizing energy storage efficiency based on changing environmental conditions.

2. Formulation of physical problem

A schematic diagram of the latent heat energy storage system (LHESS) is represented in Fig. 1. The LHESS unit is characterized by a rectangular-shaped geometry of height $H = 40$ mm and length $W = 80$ mm and the cavity has an inclination angle of θ° with the horizontal direction. The top wall is considered to be at an isothermal temperature (T_h), which varies as $\Theta = 323$ K to 343 K. All other three walls are considered to be insulated. The initial temperature of the entire system is considered as 300 K. The rectangular geometry is filled with paraffin wax PCM (RT-45). Based on the consideration, different types of nanoparticles at different concentrations are mixed with the PCM. To capture the average temperature of the PCM-filled domain, three horizontal nodal points are defined and, temperature data are stored during the analysis. The assumptions for the current work are:

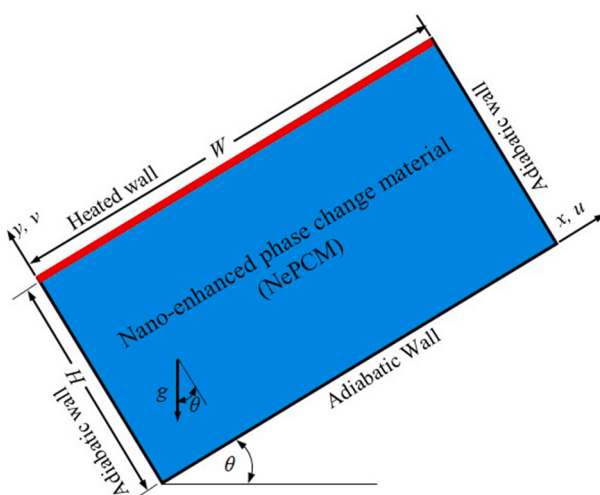


Fig. 1. Schematic diagram of the problem geometry.

- a) The heated wall is considered to be isothermal temperature ($\Theta = 323$ K to 343 K). The other walls are insulated.
- b) The adiabatic temperature of the system is set to 300 K.
- c) The density of the PCM is considered constant, and the Boussinesq approximation is used to model buoyancy effects.
- d) The problem is modeled in two dimensions, and transient phenomena are analyzed over time.
- e) The fluid properties of the PCM are considered incompressible, and the flow is assumed to be laminar.
- f) The enthalpy-porosity technique is employed to simulate the phase change, with a mushy zone constant set to $10^5 \text{ kg.m}^{-3} \text{ s}^{-1}$ to model the liquid-solid transition.
- g) The physical properties of both the PCM and nanoparticles are kept constant based on the average particle size (10–14 nm) and calculated using standard correlations.

2.1. Thermo-physical properties of PCM and nanoparticles

The thermo-physical properties of PCM (RT-45) and three different nanoparticles such as aluminum oxide (Al_2O_3), copper oxide (CuO), and Graphene nanoparticles are presented in Tables 1 and 2 respectively. Industrially available paraffin wax PCM is used for this investigation.

For the nanoparticles, the thermo-physical properties are taken at the same average particle size of 10–14 nm. Throughout all the simulations the particle size is considered to be the same. Thus the contact surface area would be the same and this will enable to compare the thermal performance of the PCM unit under different nanoparticles.

2.2. Mathematical model

For modelling the chosen problem geometry, various transport equations are employed, which describe the melting phenomena, phase change process, and heat transfer characteristics of the PCM unit. Here, the enthalpy porosity technique is employed to address or resolve the solid and melting processes of a PCM [36]. In this method, the fluid portion is considered as porous and when PCM changes its phase from solid to liquid state, porosity changes from zero to one [37]. To simplify this problem, the Boussinesq approximation is used to capture the buoyancy force [38]. The mathematical model is considered to be two dimensional and transient problems. The molten PCM liquid properties are considered to be incompressible and fluid flow to be laminar. The governing equations are given as follows [34,38,39]:

Continuity equation:

$$\frac{\partial u}{\partial x} + \frac{\partial v}{\partial y} = 0 \quad (1)$$

The momentum equations, which represent the conservation of momentum, are modified by incorporating the Boussinesq approximation to handle buoyancy effects due to temperature variations in the fluid.

Momentum equation:

x -direction:

Table 1
The thermo-physical characteristics of paraffin wax RT-45 [35].

| Properties | RT-45 |
|--|-----------------------------|
| Density (kg.m^{-3}) | 880 (solid), 770 (liquid) |
| Specific heat ($\text{J.kg}^{-1} \text{K}^{-1}$) | 3028 (Solid), 2333 (liquid) |
| Latent Heat (J.kg^{-1}) | 139,700 |
| Thermal expansion coefficient (K^{-1}) | 1.25×10^{-4} |
| Viscosity ($\text{kg.m}^{-1} \text{s}^{-1}$) | 0.0256 |
| Thermal conductivity ($\text{W.m}^{-1} \text{K}^{-1}$) | 0.2415 |
| Liquidus temperature (K) | 322 |
| Solidus temperature (K) | 308 |

Table 2

Thermo-physical property of nanoparticles [14–16].

| Chemical composition | Type of nanoparticles | | |
|---|-------------------------|--------------------------------|-------------------------|
| | CuO | Al ₂ O ₃ | Graphene |
| Density (kg.m ⁻³) | 6320 | 3900 | 2267 |
| Specific heat (J.kg ⁻¹ K ⁻¹) | 532.5287 | 800 | 700 |
| Thermal conductivity (W.m ⁻¹ K ⁻¹) | 76.5 | 46 | 5300 |
| Thermal expansion coefficient (K ⁻¹) | 0.85 × 10 ⁻⁵ | 12.66 × 10 ⁻⁶ | 1.25 × 10 ⁻⁵ |
| Morphology | Spherical | Spherical | Nano-tube |
| Particle size (nm) | 10–14 | 10–14 | 10–14 |

$$\rho \left(\frac{\partial u}{\partial t} + u \frac{\partial u}{\partial x} + v \frac{\partial u}{\partial y} \right) = \mu \left(\frac{\partial^2 u}{\partial x^2} + \frac{\partial^2 u}{\partial y^2} \right) - \frac{\partial p}{\partial x} - \frac{\mu}{k} u + A_{mush} \frac{(1-f)^2}{f^3 + \delta} u + \rho_{ref} g \beta \sin \theta (T - T_{ref}) \quad (2)$$

y- direction:

$$\rho \left(\frac{\partial v}{\partial t} + u \frac{\partial v}{\partial x} + v \frac{\partial v}{\partial y} \right) = \mu \left(\frac{\partial^2 v}{\partial x^2} + \frac{\partial^2 v}{\partial y^2} \right) - \frac{\partial p}{\partial y} - \frac{\mu}{k} v + A_{mush} \frac{(1-f)^2}{f^3 + \delta} v + \rho_{ref} g \beta \cos \theta (T - T_{ref}) \quad (3)$$

This momentum equation is on the basis of the Boussinesq hypothesis and the Buoyancy - driven convection is simulated with the Boussinesq approximation [40]. In the Boussinesq approximation, the density of the fluid is taken as constant for all the equations except the body force term. These two $\frac{\mu}{k} u$ and $\frac{\mu}{k} v$ terms are the viscous loss term of the right side of Eqs. (2) and (3), which are added due to the porous model consideration [41]. This term is used for distinguishing the PCM region from the solid surface for the momentum eq. PCM region $1/k$ is set to zero. For the enthalpy-porosity model, a fourth term will be added on the right side of Eqs. (2) $A_{mush} \frac{(1-f)^2}{f^3 + \delta} u$ and Eq. (3) $A_{mush} \frac{(1-f)^2}{f^3 + \delta} v$. Where, the liquid volume fraction is taken as f , and the mushy zone constant is taken as A_{mush} . These two porosity function terms, which were developed by Brent et al. [42], are what cause momentum equations to resemble Carman-Kozney equations for flow in a porous media.

The Boussinesq hypothesis:

$$(\rho - \rho_{ref}) g = -\rho_{ref} \beta (T - T_{ref}) \quad (4)$$

where, ρ_{ref} is reference density, T_{ref} is the reference temperature, and β the volumetric expansion coefficient.

To simulate the solid-liquid phase change of the PCM, the enthalpy-porosity technique is used. This model treats the mushy zone (the region where both solid and liquid phases coexist) as a porous medium.

$$f = \begin{cases} f = 1, & T > T_m \\ \frac{T - T_s}{T_m - T_s}, & T_s < T < T_m \\ f = 0, & T < T_s \end{cases} \quad (5)$$

In Eq. (5) the description of f is given. For the above numerical simulation, the value of the A_{mush} constant is taken as $10^5 \text{ kg.m}^{-3} \text{ s}^{-1}$, which has been evaluated by the mushy zone constant independent test. When $f = 0$, then the δ comes into account to avoid the division by zero. Where δ is nothing but a tiny constant number (0.001). The natural convection is denoted by the fifth term on the right side of Eq. (3).

Energy equation:

$$(\rho C_p)_{PCM} \left[\frac{\partial T}{\partial t} + u \frac{\partial T}{\partial x} + v \frac{\partial T}{\partial y} \right] = K_{PCM} \left(\frac{\partial^2 T}{\partial x^2} + \frac{\partial^2 T}{\partial y^2} \right) - \left[\frac{\partial}{\partial t} (\rho \Delta h) + u \frac{\partial}{\partial x} (\rho u \Delta h) + v \frac{\partial}{\partial y} (\rho v \Delta h) \right] \quad (6)$$

In Eq. (6) K_{PCM} is represented as the thermal conductivity of PCM. The total enthalpy can be described as the sum of sensible heat capacity and the latent heat of phase change. This concept is formally defined as:

$$\Delta h = h + L \quad (7)$$

The calculated enthalpy is outlined as follows:

$$h = h_{ref} + \int_{T_{ref}}^T C_p dT \quad (8)$$

here, ' h_{ref} ' represents the sensible enthalpy of PCM at a reference temperature denoted as ' T_{ref} '.

The initial condition for this present work: at, $t = 0$, $T = 300 \text{ K}$.

The imposed boundary conditions for the chosen problem are:

T_h = heated top wall with constant temperature (isotherm wall) of $\Theta = 343 \text{ K}$.

$T_{adiabatic}$ = three sides are adiabatic with a temperature of 300 K which is the same as the initial temperature as well as the adiabatic temperature and heat flux 0 W/m^2 .

No slip boundary condition is considered at the walls, $u = v = 0$.

2.3. Thermo-physical property calculation of NePCM

In general, the thermal conductivity is low for a pure PCM, so the thermal energy storage or recovery of the stored energy is slower for a limited time frame. The thermal conductivity of the PCM unit can be enhanced by mixing the appropriate type and concentration of nanoparticles with pure PCM. With is mixing, the value of thermal conductivity changes, and all the other thermo-physical properties also change, which directly influences the total melting time of the NePCM. Thus for the analysis, all the thermo-physical properties are calculated using the standard correlations [43–46]. The predicted thermo physical properties of the samples are calculated based on the corresponding volume fraction of the nanoparticles. These are the following Equations:

a) The density of the NePCM was evaluated by [47],

$$\rho_{nano-PCM} = (1 - \varphi) \rho_{PCM} + \varphi \rho_{nanoparticles} \quad (9)$$

where φ is represented the volume fraction of the nanoparticles.b) The specific heat capacity (C_p) of NePCM is defined by [47],

$$C_{P_{nano-PCM}} = \frac{(1 - \varphi) (C_p)_{PCM} + \varphi (C_p)_{nanoparticles}}{\rho_{nano-PCM}} \quad (10)$$

c) The thermal conductivity of the nano-PCM is defined by, the thermal conductivity due to the addition of nanoparticles in pure PCM (NePCM) was determined using the model of Maxwell [48]:

$$K_{nano-PCM} = K_{PCM} \left[\frac{(2K_{PCM} + K_{nanoparticles}) - 2\varphi(K_{PCM} - K_{nanoparticles})}{(2K_{PCM} + K_{nanoparticles}) - \varphi(K_{PCM} - K_{nanoparticles})} \right] \quad (11)$$

where K represents the thermal conductivity.

d) The viscosity is calculated from the Maxwell equation, and the viscosity of the nano-PCM can be obtained using the extended equation of Einstein by Brinkman as follows [49]:

$$\mu_{nano-PCM} = \frac{\mu_{PCM}}{(1 - \varphi)^{2.5}} \quad (12)$$

e) The thermal expansion coefficient of the nano-PCM is calculated from [35]

$$\beta_{\text{nano-PCM}} = \frac{(1 - \varphi)(\rho\beta)_{\text{PCM}} + \varphi(\rho\beta)_{\text{nano-particles}}}{\rho_{\text{nano-PCM}}} \quad (13)$$

where β represented as the thermal expansion coefficient.

f) The latent heat of the nano-PCM is calculated by [49],

$$L_{\text{nano-PCM}} = \frac{(1 - \varphi)(\rho L)_{\text{PCM}}}{\rho_{\text{nano-PCM}}} \quad (14)$$

where L represents the latent heat of fusion and ρ represents the density.

The melting speed of PCM can be determined by measuring the time taken for the PCM to completely melt under controlled conditions.

Melting speed:

The melting speed is calculated as:

$$\text{Melting speed} = \frac{\text{Total mass of PCM}}{\text{Total time to melt}} \quad (15)$$

Total mass of the PCM = total volume \times density of the PCM

Another way to measure the melting speed is if the volume fraction of liquid PCM is being monitored, the speed can be expressed in terms of the increase in liquid fraction per unit time.

Energy storage rate:

The energy storage capacity of a PCM can be evaluated using the latent heat of fusion and the mass of the PCM [50]. The steps are as follows:

Find the latent heat of fusion (L) for the PCM, typically expressed in joules per kilogram (J/kg). Measure the mass (in kg or g) of the PCM being used. The total energy storage capacity (Q) can be calculated using the formula:

$$Q = m \times L \quad (16)$$

Energy storage rate:

$$\text{Energy storage rate} = \frac{\text{Total energy storage}}{\text{Total time to melt}} \quad (17)$$

This equation gives the amount of energy (in joules) that can be stored during the phase transition from solid to liquid.

Enhancement parameter

The enhancement parameter typically refers to the improvement in thermal performance due to the addition of nanoparticles. This can be assessed using various metrics, such as thermal conductivity, heat transfer rates, energy storage efficiency or total melting time. The following is a method for determining it:

The enhancement can be calculated as:

Enhancement parameter =

$$\frac{\text{Total melting time without nanoparticles} - \text{Total melting time with nanoparticles}}{\text{Total melting time without nanoparticles}} \times 100\% \quad (18)$$

In this investigation, all the thermo physical properties are calculated for different volume fractions of the nanoparticles and that is up to 5 % by the above equations. It should be noted that in reality, a small amount of sedimentation can be observed after volume fraction $\varphi = 3\%$.

3. Solution methodology

3.1. Numerical method

The involved mathematical models are solved numerically by double precision and parallel as processing options with 4 processors as solvers [51]. The Ansys Fluent solver is based on a pressure-based solver with absolute velocity formulation [52]. It is a transient problem so the transient solver is selected with planner 2D space and the value of gravity is selected as -9.81 m/s^2 in y direction. For solving the transient models, the working medium is considered as laminar, and viscous. The PCM is defined by its various properties based on the considered cases. It is assumed that the PCM density remained constant, specifically at the solidus temperature. Employing the Boussinesq approximation, the analysis accounted for the buoyancy effect. The approach adopted for solving the mathematical model, the SIMPLE scheme coupled with pressure and velocity is adopted. For addressing the pressure correlation equation, the PRESTO! is applied, which is very useful for the simulation of thermal convection-based problems [53]. The second-order upwind scheme is selected for the spatial discretization of the energy and momentum equation. Frist Order Implicit scheme is adopted for the transient formulation [54]. The relaxation coefficients for density, body force, liquid fraction, velocity, pressure, and energy are assigned as 1, 1, 0.9, 0.7, 0.3, and 1 respectively. The absolute convergence criteria for the continuity is taken as 10^{-6} (along the x -velocity, y -velocity equation), and 10^{-10} is considered as absolute convergence criteria for the energy Eq. [55]. The solution initialization typically employs standard initialization. In this case, the time step size (s) is set to the optimal value of 0.5 s, and 140 number of iterations are used per time step. The governing equations are solved using Computational Fluid Dynamics (CFD) with the finite volume method. The solution uses the Semi-Implicit Method for Pressure-Linked Equations (SIMPLE) algorithm [56]. A second-order upwind scheme is applied to the energy and momentum equations to improve accuracy. The time-dependent nature of the problem is solved using an implicit time-stepping scheme with a time step size of 0.5 s and 140 iterations per time step.

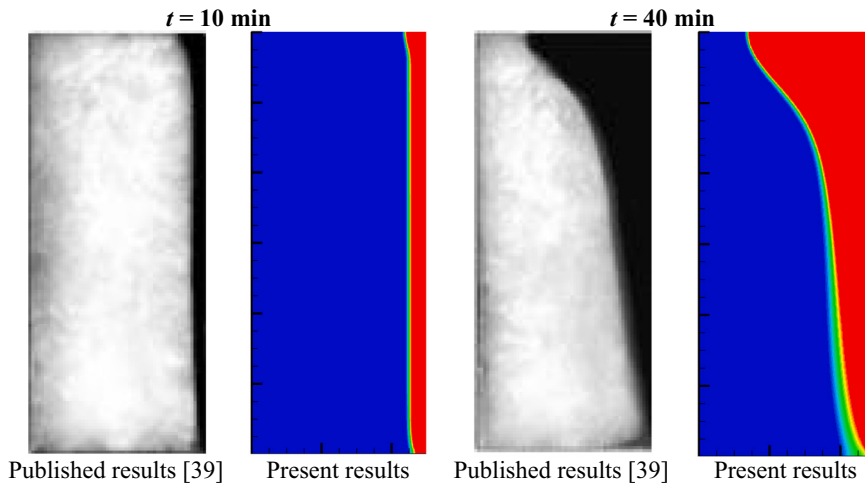
3.2. Grid and time independence test

The numerical simulation is conducted in a 2D geometry. The domain of the pure PCM-filled cavity is divided into smaller mesh. The quadrilateral cell mesh has been chosen for the present geometry. For the mesh independence test, 8 grid sizes are taken into consideration, these are 8×4 , 20×10 , 40×20 , 80×40 , 120×60 , 160×80 , 200×100 , and 240×120 . The summary of the mesh-independence study is

presented in Table 3. From all the grid sizes 160×80 with 13,041 number of nodes and 12,800 number of elements show more accuracy of the solution and time duration for each solution. Following the grid independence analysis, a time independence test is also carried out using six distinct time step intervals, namely 5 s, 2 s, 1 s, 0.5 s, 0.2 s, and 0.1 s. From these 0.5 s is the Ideal for achieving the maximum benefit. For the liquid-solid interface mushy zone parameter independence study has been conducted with 5 different mushy zone parameter constants likely they are 1×10^5 , 2×10^5 , 3×10^5 , 4×10^5 , and 5×10^5 . As a result, we have observed that there is consistency in the total duration of the melting process so we consider mushy zone constant 1×10^5 as an

Table 3Mesh independence study for $\theta = 0^\circ$ and $\Theta = 343$ K with pure PCM (RT-45).

| Criteria | | Cases | | | | | | | | | |
|---|-------|--------|--------|--------|---------|--------|--------|------------|--------|------------|--------|
| | | 1 | 2 | 3 | 4 | 5 | 6 | 7 | 8 | 9 | 10 |
| Number of Divisions | Width | 8 | 20 | 40 | 60 | 80 | 120 | 160 | 200 | 240 | 280 |
| | Depth | 4 | 10 | 20 | 30 | 40 | 60 | 80 | 100 | 120 | 140 |
| No of Nodes | | 45 | 231 | 861 | 1891 | 3321 | 7381 | 13,041 | 20,301 | 29,161 | 39,621 |
| No of Elements | | 32 | 200 | 800 | 1800 | 3200 | 7200 | 12,800 | 20,000 | 28,800 | 39,200 |
| Total melting time (s) | | 20,506 | 20,347 | 20,320 | 203,011 | 20,304 | 20,301 | 20,300 | 20,299 | 20,299 | 20,299 |
| Time deflection from optimum value (s) | | 207 | 48 | 21 | 12 | 5 | 2 | 1 | 0 | 0 | 0 |
| average time taken for every 5 min solution | | 5 min | 10 min | 20 min | 30 min | 40 min | 1 h | 1 h 20 min | 2 h | 2 h 40 min | 4 h |

**Fig. 2.** Validation of the present computing technique through the comparison of liquid fraction with respect to different time steps ($t = 10$ and 40 min) with published experimental results of Kamkari and Shokouhmand [39] with a cavity inclination of $\theta = 90^\circ$.

optimum value.

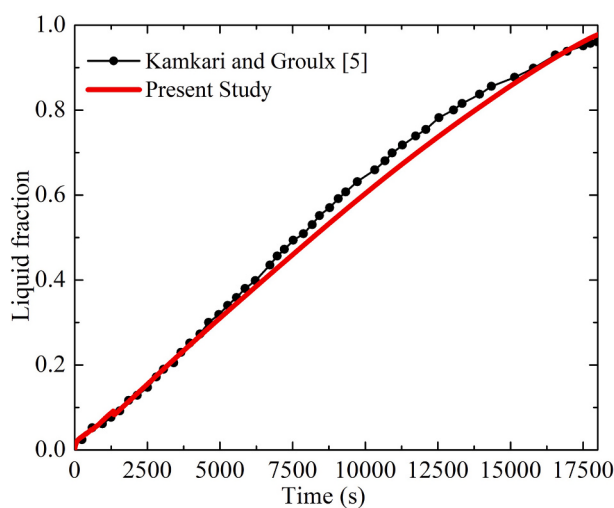
3.3. Validation study

Before conducting extensive simulation, the present computing technique is tested to evaluate the accuracy. This is done by validating the published problem. For the initial validation of the developed model, the experimental model of Kamkari and Shokouhmand [39] is simulated. The problem geometry comprises finned rectangular enclosures

filled with lauric acid PCM under different inclination angles. The base is 50 mm long, and the height is 120 mm. The rectangle-enclosed system is exposed to constant thermal conditions ($\Theta = 70$ °C) at one side of the vertical wall, considering all the other sides are adiabatic with a 90° inclination angle (θ). The numerical examination occurs within a two-dimensional space featuring a geometry mirroring that of the experimental setup. The same PCM properties have been used for the numerical validation. Validation of the present computing technique through the comparison of liquid fraction contour with respect to different time frames with published experimental results of Kamkari and Shokouhmand [39] shown in Fig. 2. Furthermore, another validation study is conducted by simulating the problem of Kamkari and Groulx [5] with a cavity inclination of $\theta = 90^\circ$ and $\Theta = 60$ °C. Corresponding liquid fraction with time is also plotted in Fig. 3, which is demonstrated a strong alignment with the published experimental results (with an error level < 3 %) of Kamkari and Groulx [5]. This comparison shows the excellent accuracy of the present computing technique.

4. Assessments of the results

This work numerically explores the influence of different types and concentrations of nanoparticles (namely, Al_2O_3 , CuO , and Graphene) on the melting performance of paraffin wax-filled inclined rectangular thermal systems. The study found out the effect of different nanoparticles on the melting speed and, thus, the amount of energy stored. The length of the heated surfaces and the size of the container are kept constant throughout the analysis. This research delves into the impact of various nanoparticles specifically, Al_2O_3 , CuO , and Graphene for the different concentrations $\varphi = 0.5\%$, 1% , 2% , 3% , 4% and 5% , on both melting rates and total melting times. Additionally, it explores the influence of inclination angles ranging from $\theta = 0^\circ$ to 60° and hatted wall

**Fig. 3.** Validation of the present computing technique through the comparison of liquid fraction with respect to time with published experimental results of Kamkari and Groulx [5] with a cavity inclination of $\theta = 90^\circ$ and $\Theta = 60$ °C.

temperatures ranging from $\Theta = 323$ K to 343 K on the thermal characteristics of the most effective nanoparticle type with the correct volume fraction.

4.1. Melting behavior of NePCMs with different nanoparticles

As the upper wall is subjected to isothermal heating and the rest of the walls are adiabatic, the melting process is initiated from the adjacent layer of the upper solid wall and then propagates in the downward direction. In this way, solid PCM is transformed into liquid PCM. Thus, liquid fraction increases gradually with the progress in time. During the initial time step, heat is transferred very fast (through conduction mode) from the heated wall to the adjacent solid PCM, and a thin layer of liquid PCM is formed. After some time, the volume of liquid PCM in between the solid heated surface and solid PCM increases and thus the solid-liquid interface shifts downward. In the presence of heated liquid PCM, the convective heat transfer starts to play and dictates the heat transfer process. Therefore, the buoyancy effect dominates the heat transfer process as well shifting of the solid-liquid interface.

4.1.1. Temporal evolution of melting process

The temporal evolution of the melting process provides valuable insights into the behavior of PCMs during thermal energy storage applications. By analyzing liquid fraction and temperature contours over time, we aim to understand how the PCM transitions from a solid to a liquid state and how thermal energy is absorbed and distributed throughout the material during this transformation as shown in Fig. 4 for the pure PCM, $\theta = 0^\circ$, $\Theta = 343$ K. This investigation sheds light on the dynamic behavior of PCMs, which is essential for optimizing their performance in various thermal energy storage systems.

At a zero-degree inclination angle, conduction is the dominant mode of heat transfer initially, as the heated top wall directly transfers thermal energy to the adjacent solid PCM through conduction. This is evident in the early stages, where a thin layer of liquid PCM forms at the interface between the heated wall and the solid PCM, allowing heat to penetrate through the solid material. As the melting process progresses, natural convection (free convection) begins to play a significant role. Once a sufficient volume of the PCM melts and forms a liquid layer, buoyancy effects start to develop due to temperature differences within the liquid PCM. This transition signifies the onset of natural convection, which enhances heat transfer by promoting fluid motion and facilitating a more uniform temperature distribution throughout the PCM. At the zero-degree angle, while conduction remains important during the initial phase of melting, free convection becomes increasingly influential

as more of the PCM transitions to the liquid state.

During the initial stage at $t = 0$ to 10 min, the PCM remains solid, exhibiting a liquid fraction of 0 throughout its structure. Temperature contours uniformly depict temperatures below the melting point of the material. As the early melting phase ensues at $t = 20$ min, melting initiates at the interface where the temperature surpasses the melting point, gradually increasing the liquid fraction in proximity to this interface. Correspondingly, temperature contours reveal a gradient from the heat source towards the PCM, with areas adjacent to the heat source reaching the melting temperature of 343 K. As intermediate melting progresses at $t = 70$ min, the liquid fraction continues to rise, signifying a greater portion of the PCM transitioning into the liquid state. Temperature gradients persist, though more of the PCM now reaches the melting temperature, evidenced by larger areas exhibiting 343 K temperature contours. Advancing to the advanced melting stage at $t = 130$ min, a significant portion of the PCM has melted, leaving behind a minor solid core amidst a higher liquid fraction throughout the material. Temperature contours illustrate that almost half of the PCM now hovers around or at 340 K, with only central or distant areas from the heat source retaining cooler temperatures. Finally, the PCM completely liquefies upon complete melting, resulting in a liquid fraction of 1 throughout the material. This is evidenced by uniformly 343 K temperature contours that span the entire PCM.

In the visual representation of the melting process shown in Fig. 4, the liquid fraction and temperature contours provide insights into the temporal evolution of the thermal state of PCM. Initially, the liquid fraction is at its lowest, indicating a solid PCM. As melting commences, the liquid fraction gradually increases near the heat source, marking the early melting stage. Throughout the intermediate melting stage, this fraction continues to rise, spreading outward from the heat source. In the advanced melting stage, a significant portion of the PCM has transitioned to the liquid state, leaving only a small solid core. Finally, as the process concludes, the liquid fraction reaches its maximum value of 1, indicating complete liquefaction of the PCM. Concurrently, the temperature contours exhibit a corresponding progression. Initially, temperatures are uniformly below 343 K. However, as melting initiates, a temperature gradient forms, with regions near the heat source reaching higher temperatures. This gradient expands during intermediate melting, encompassing larger areas of the PCM. In the advanced melting stage, most of the PCM nears the melting temperature. Ultimately, with complete melting, the entire PCM reaches a uniform temperature of $\Theta = 343$ K. These visual representations elucidate the dynamic nature of the melting process and provide valuable insights into the thermal behavior of the PCM shown in Fig. 4.

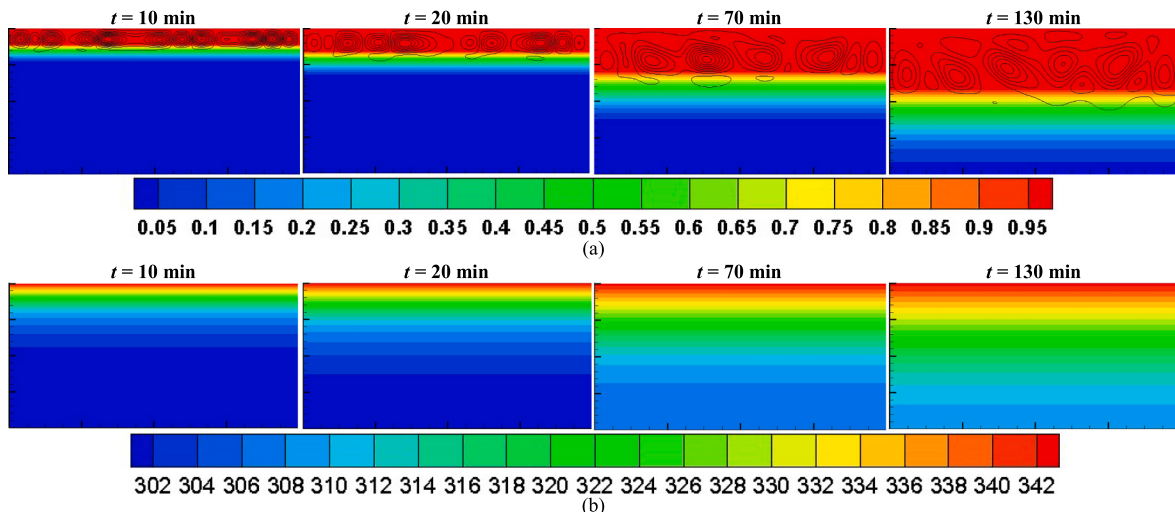


Fig. 4. Temporal evolution of melting process using (a) liquid fraction (f), and (b) temperature contours for the pure PCM, $\theta = 0^\circ$, $\Theta = 343$ K.

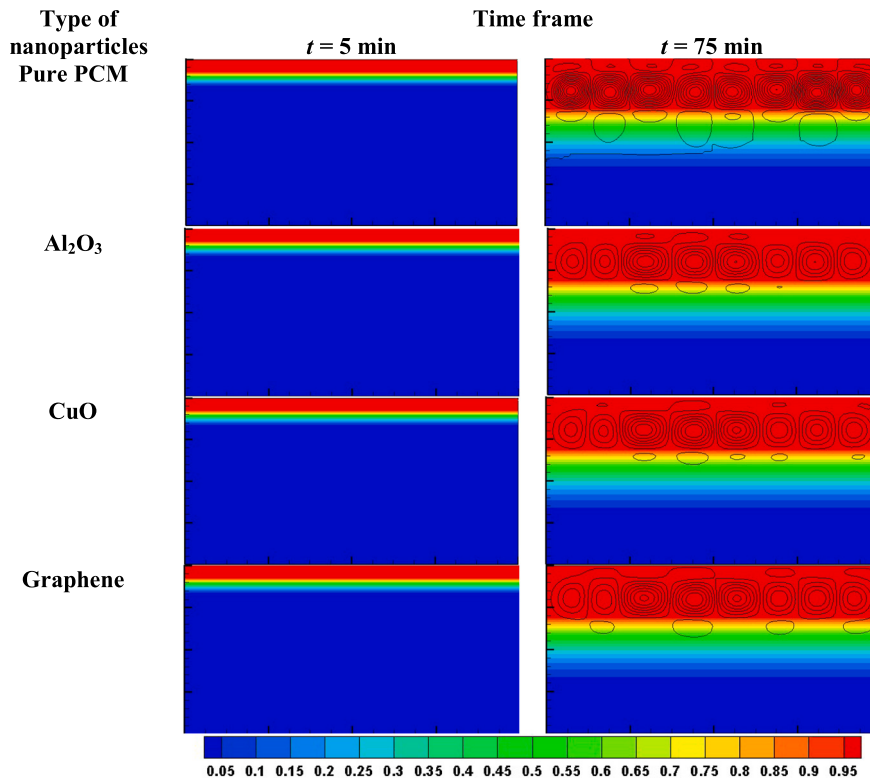


Fig. 5. Liquid fraction contours at $t = 5 \text{ min}$ and 75 min for Al_2O_3 , CuO , and Graphene nanoparticles at $\varphi = 0 \%$ and $\varphi = 2 \%$ when $\theta = 0^\circ$, $\Theta = 343 \text{ K}$.

4.1.2. Initial and steady-state melting characteristics

At the initial stages of melting ($t = 5 \text{ min}$), the introduction of nanoparticles does not significantly influence the melting characteristics of the NePCMs as the heated surface is in direct contact with the solid

PCM or NePCM.

The liquid fraction Fig. 5 provides a comprehensive comparison of liquid fraction contours and streamlines across two distinct time steps $t = 5 \text{ min}$ and 75 min under the three different types of nanoparticles

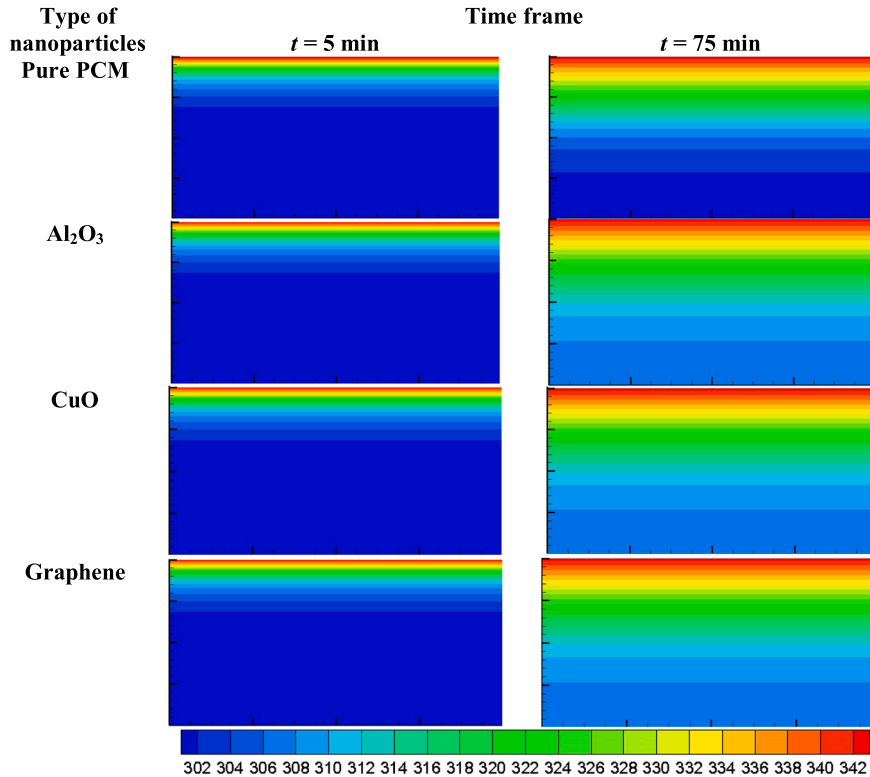


Fig. 6. Temperature profiles at $t = 5 \text{ min}$ and 75 min for Al_2O_3 , CuO , and Graphene nanoparticles at $\varphi = 0 \%$ and $\varphi = 2 \%$ when $\theta = 0^\circ$, $\Theta = 343 \text{ K}$.

(Al_2O_3 , CuO , and Graphene in row-wise) with a constant volume fraction of $\varphi = 0\%$ and 2% . For the comparison, contours of liquid fraction in the absence of nanoparticles ($\varphi = 0\%$) are presented. The color gradient utilized in the contour plots corresponds to the distribution of liquid fraction, with red representing pure liquid (liquid fraction $f = 1$) and blue representing pure solid (liquid fraction $f = 0$). The intermediate region between solid and liquid phases is referred to as the mushy zone, where solid PCM to liquid PCM transitions occur.

From Fig. 5, it is observed that for $t = 5$ min, a thin layer of liquid PCM is formed in the upper most regions of the cavity. Furthermore, a notable observation is that the solid-liquid interface exhibits a slightly more downward movement in the presence of nanoparticles compared to the case of no nanoparticles. This movement manifests as a downward linear progression of the solid-liquid interface. Initially, the interface experiences rapid propagation (due to conduction heat transfer), which gradually slows down over time (due to convection). Moreover, the thickness of the mushy zone increases progressively as the time frame extends from $t = 5$ min to 75 min. Therefore, this comparison clearly demonstrates the beneficial effect of nanoparticle inclusion in the PCM, which enhances the melting process.

Although the temperature contours as in Fig. 6 for $t = 5$ min may not exhibit discernible differences visually, the contours for $t = 75$ min clearly depict the variations in the average temperature of the PCM domain. At $t = 5$ min, with conduction prevailing, minimal alterations in the isotherm lines are observable, particularly evident in the case of Al_2O_3 . However, CuO and Graphene display slight deviations in the isotherm lines. By the $t = 75$ min, with convection taking precedence in heat transfer, the spread of isotherm lines becomes apparent across the three nanoparticle varieties when contrasted with pure PCM. Nevertheless, the variance in propagation among the nanoparticles remains insignificant. Upon initiation during the melting procedure, a fragile stratum of liquefied substance forms accompanied by minuscule vortices symmetrically emerge around the nascent melted layer due to conduction. Subsequently, as time progresses, the temperature of the PCM in the molten area increases, facilitating the dominance of natural convection in this zone. Consequently, the convective shell rebounds from the upper surface, inducing a downward expansion of the melted zone. These diminutive vortices amalgamate over time, culminating in the formation of a more substantial convective shell, as depicted in Figs. 5 and 6. This distinction becomes evident when comparing the local temperature contours of $\varphi = 2\%$ nanoparticles concentration with the no-nanoparticles. The temperature contours highlight the evolving thermal behavior of the system over time. It also demonstrates the higher temperature magnitudes in the presence of nanoparticles. This is due to the increase in the effective thermal conductivity of the PCM domain, which allows faster heat transfer from the heating surface to the solid PCM. Such insights contribute to a deeper understanding of the temporal evolution of phase change processes and the influence of nanoparticles on thermal performance.

In the melting behavior of NePCMs with different nanoparticles, the melting process is primarily influenced by the enhanced thermal properties introduced by the nanoparticles. Initially, heat is transferred through conduction from the heated wall to the adjacent PCM, causing a thin layer of liquid to form at the solid-liquid interface. As the melting progresses, the buoyancy-driven natural convection within the liquid PCM becomes more significant, accelerating the heat transfer process. The addition of nanoparticles, such as Al_2O_3 , CuO , and Graphene, increases the thermal conductivity of the PCM, promoting faster heat transfer. Graphene nanoparticles, in particular, with its exceptionally high thermal conductivity, drastically improves the melting rate compared to the other nanoparticles. As the liquid layer grows, the convective currents strengthen, further enhancing the melting dynamics. But higher nanoparticle concentrations might cause an increase in viscosity, slowing natural convection and perhaps affecting melting rate. Ultimately, the melting process is driven by the combination of conduction, convection, and increased thermal conductivity from

nano-particles, with different nanoparticles resulting in varying degrees of thermal performance enhancement.

4.2. Influence of nanoparticle concentration

4.2.1. Temporal evolution of liquid fraction

The temporal evolution of the liquid fraction demonstrates how different concentrations of nanoparticles impact the melting process. Higher concentrations result in a more rapid increase in the liquid fraction, indicating a faster melting rate. This acceleration is due to the enhanced thermal conductivity provided by the nanoparticles, which facilitates more efficient heat transfer throughout the PCM. Consequently, the material melts more uniformly and quickly at higher nanoparticle concentrations. Conversely, lower concentrations of nanoparticles lead to slower melting and more pronounced temperature gradients within the PCM. This analysis highlights the importance of optimizing nanoparticle concentration to achieve efficient and uniform melting in NePCMs for thermal energy storage applications.

Fig. 7 delves the liquid fraction over increasing time steps, which examines various percentages of Al_2O_3 , CuO , and Graphene nanoparticles—ranging from $\varphi = 0.5\%$ to 5% volume fraction—compared to a scenario without nanoparticles ($\varphi = 0\%$). In general, the liquid fraction (f) increases with the progress in time. Upon closer inspection of Fig. 7(b), the enhanced view of the liquid fraction plot reveals a notable trend, the nanoparticle concentration $\varphi = 5\%$ exhibits a faster melting process. Analyzing the results, it is observed intriguing nuances: for instance, the melting time for $\varphi = 0.5\%$ Al_2O_3 surpasses that of $\varphi = 1\%$, aligning closely with the duration observed for $\varphi = 2\%$ nanoparticle concentration. This trend holds true for both CuO and Graphene nanoparticles in Fig. 7(c,d) and (e,f) respectively. Clearly, a higher mass fraction correlates with accelerated melting rates, leading to shorter total melting time. This phenomenon can be attributed to the combined effects of reduced latent heat of fusion and augmented thermal conductivity. As the nanoparticle mass fraction increases, the specific heat of the NePCM decreases, while its thermal conductivity and density rise. Consequently, the addition of nanoparticles diminishes the overall latent heat required for complete melting. The latent heat of fusion is the energy required to change a substance from solid to liquid at its melting point without altering its temperature. When nanoparticles are incorporated into the PCM, they disrupt the molecular structure and interactions within the material, often resulting in a decrease in the latent heat of fusion.

It is worth noting that as the volume fraction of nanoparticles escalates, so does the viscosity of the NePCM, potentially impeding the heat transfer process. However, the reduction in melting time underscores the dominant influence of factors conducive to melting, such as heightened conductivity and reduced latent heat, outweighing the adverse effects of viscosity. This intricate interplay highlights the multifaceted dynamics at play in nanoparticle-enhanced phase change materials.

4.2.2. Temperature distribution analysis

The temperature distribution at various nanoparticle concentrations shows that the inclusion of nanoparticles significantly affects the thermal behavior of the PCM. Higher concentrations of nanoparticles result in more uniform temperature distribution throughout the material. This uniformity is attributed to the enhanced thermal conductivity provided by the nanoparticles, which facilitates more efficient heat transfer. At lower nanoparticle concentrations, temperature gradients are more pronounced, indicating slower heat diffusion. This analysis underscores the importance of optimizing nanoparticle concentration to achieve optimal thermal performance in NePCMs for thermal energy storage applications.

For a better understanding of the thermal behavior of the PCM domain, the temperature variations at different nodal points are analyzed. Here three nodal points (T_1 , T_2 , and T_3) are defined with the

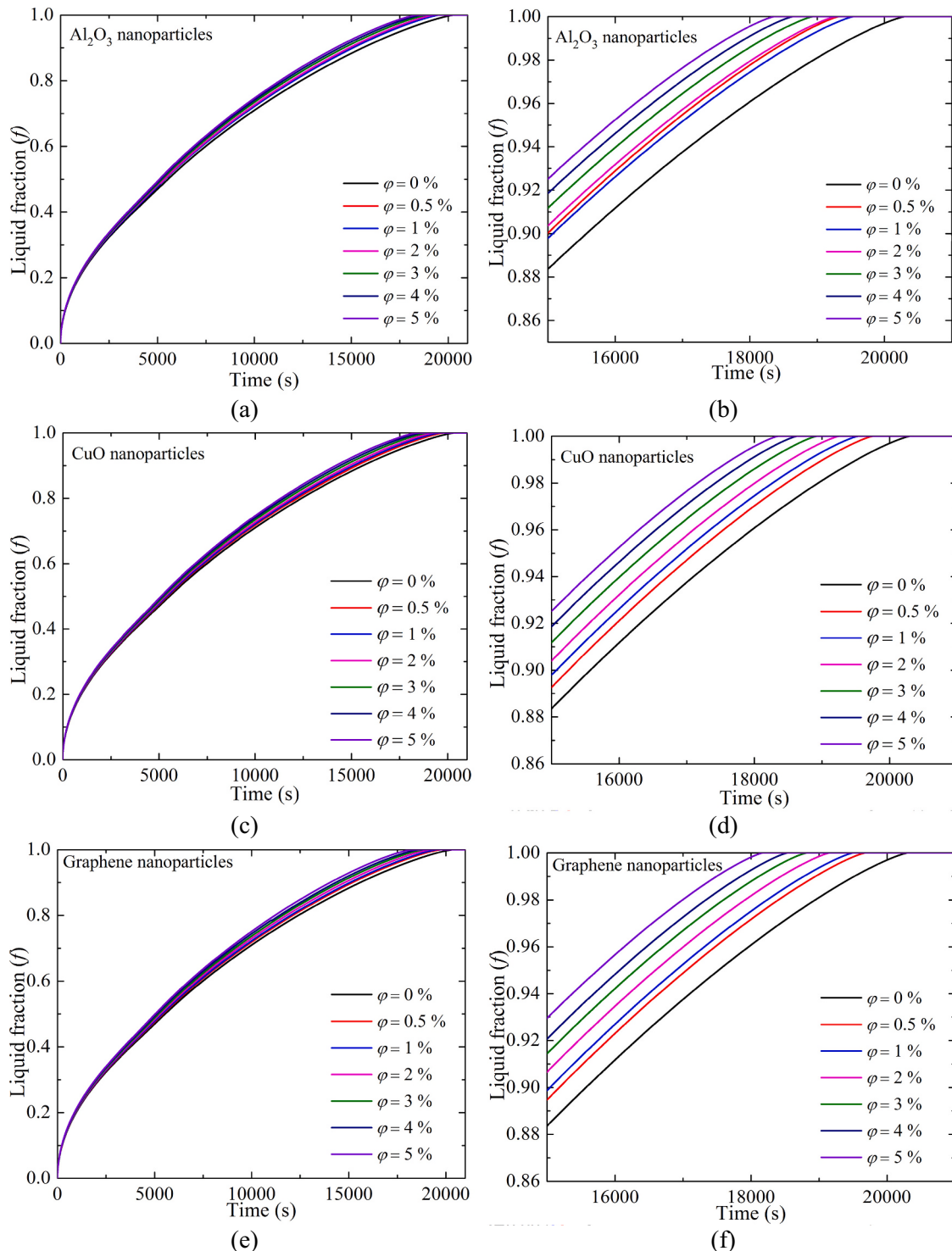


Fig. 7. The liquid fraction (f) with different concentrations of (a and b) Al_2O_3 , (c and d) CuO , and (e and f) Graphene nanoparticles varying their concentrations ($\varphi = 0.5\% \text{ to } 5\%$) when $\theta = 0^\circ$, $\Theta = 343\text{ K}$.

coordinates (40, 38; 40, 20; 40, 2) of the PCM domain (all units of the coordinates are in mm) as shown in Fig. 8. The temperature profile of the nodal points offers additional precise data, which are necessary to look at how nanoparticles affect both the kinetic and thermal behavior of the melting process. Fig. 9 demonstrates the temperature at different nodal points of the PCM domain with the consideration of Al_2O_3 , CuO , and Graphene nanoparticles when the hot wall temperature is kept at 343 K. The transfer of thermal energy through the solid state of the material causes the nodal points temperature to rise initially for all the

concentration nanoparticles until the melting point is reached, thereby conducting heat transport to the solid PCMs. The first row of the nodal points has an exponential growth rate of temperature that is substantially higher than the second and third rows during the melting process. This can be clarified through the simple fact that substantial heat conduction through the thin layer of liquid PCM surrounds the first column of nodal points and transfers heat to the solid PCM from the top heated wall. It is important to note that the thin layer of liquid PCM is the sole area in which heat transmission by conduction is dominated over

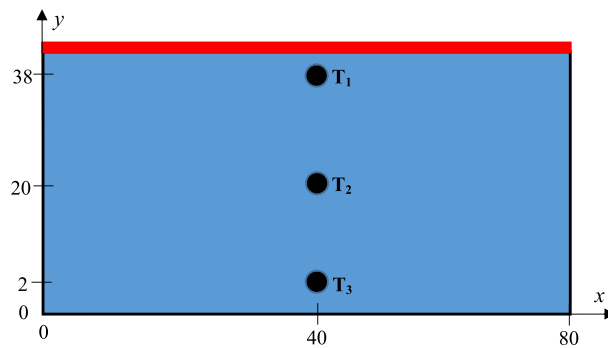


Fig. 8. Nodal points of the schematic diagram.

convection. After a few times first row of nodal points increase exponentially and get a steady temperature at $\Theta = 343$ K. For the second nodal point row temperature increases with positive decreasing curve characteristics. This indicates that convection starts to dominate conduction. The temperature of the third layer of nodal point initially increases, after some time degree of temperature increase reduces and after that, it again increases. This indicates first increment was sensible heating; the second increment was latent heat donation and the third one again sensible heat as the PCM for the third layer of nodal points melted. The liquid PCM temperatures near the border of the thermal boundary layer are related to these nodal points' layer temperatures. The existence of an anticlockwise rotational flow in the fluid is confirmed by the observed pattern of dropping temperatures from the top to lower nodal points, which suggests the development of the thermal boundary layer that lies along this interface.

Fig. 10 presents a detailed analysis of the impact of different types of nanoparticles and their concentrations on the liquid fraction throughout the melting process, with an enlarged view covering the time range from 15,000 s to 21,000 s and liquid fraction from 0.85 to 1. The findings reveal a notable positive influence of increasing the concentration of nanomaterials, namely Al_2O_3 , CuO , and Graphene, on the melting process, leading to a reduction in the liquid fraction at specific time intervals. A consistent trend is observed with any type of nanoparticles, indicating their effectiveness in enhancing the melting behavior of the PCM. Specifically, Fig. 10 (a) illustrates the results for $\varphi = 0.5\%$ volume fraction of the three nanoparticles compared with pure PCM ($\varphi = 0\%$). Notably, Al_2O_3 nanoparticles demonstrate the highest reduction in melting time compared to CuO and Graphene at this concentration ($\varphi = 0.5\%$). Upon increasing the volume fraction to 1 %, a further reduction in total melting time is observed compared to the 0.5 % volume fraction. Notably, Graphene exhibits the most significant reduction in total melting time among the three nanoparticles. Additionally, a merging of the liquid fraction plotted curves for CuO and Al_2O_3 nanoparticles is observed, indicating similar performance trends. This trend persists for volume fractions of $\varphi = 2\%$ and 3% , where Graphene continues to demonstrate the highest reduction in total melting time compared to CuO and Al_2O_3 nanoparticles. However, at a nanoparticle concentration of $\varphi = 4\%$ by volume, while growth in the liquid fraction is observed, the reduction in total melting time remains consistent across all three nanoparticles. Thus, the choice of nanoparticle type becomes insignificant at this concentration level. Similarly, at a concentration level of $\varphi = 5\%$ by volume, growth for the liquid fraction occurs, but the reduction in total melting time remains consistent for CuO and Al_2O_3 nanoparticles. Remarkably, Graphene nanoparticles consistently exhibit the highest reduction in total melting time across all volume fractions, showing their superior effectiveness in enhancing the melting process of the PCM. In summary, Fig. 10 provides valuable insights into the nuanced effects of nano-additives and their concentrations on the melting behavior of PCM, highlighting the significant potential of Graphene nanoparticles for optimizing thermal energy storage systems.

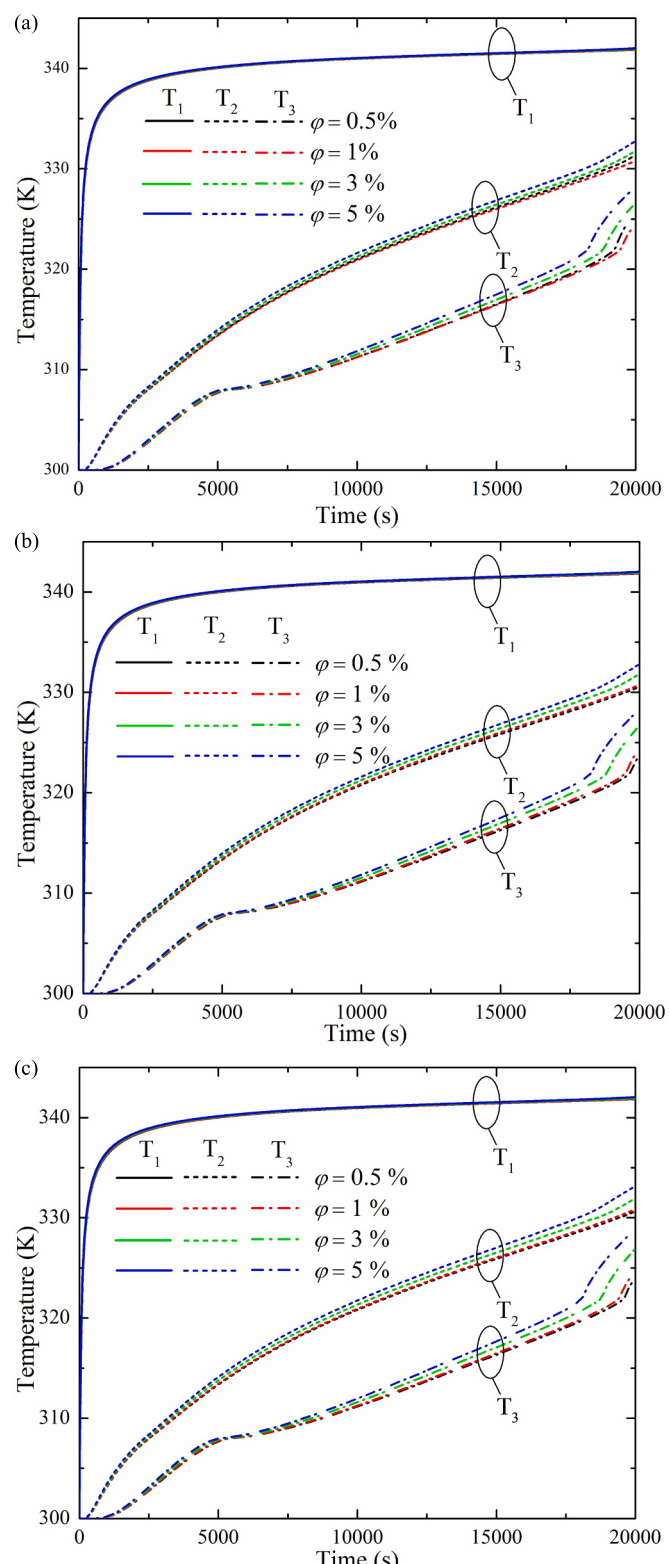


Fig. 9. Temperature distribution with different concentrations of (a) Al_2O_3 , (b) CuO , and (c) Graphene nanoparticles ($\varphi = 0.5\%$ to 5%) when $\theta = 0^\circ$, $\Theta = 343$ K.

It is pertinent to mention that the thermo-physical properties of nanomaterials have a significant impact on identifying the cause of different thermal behaviors of the NePCM. Although CuO has the highest density (6320 kg/m^3) among Al_2O_3 (3900 kg/m^3) and Graphene (2267 kg/m^3), Graphene nanoparticles has the highest thermal

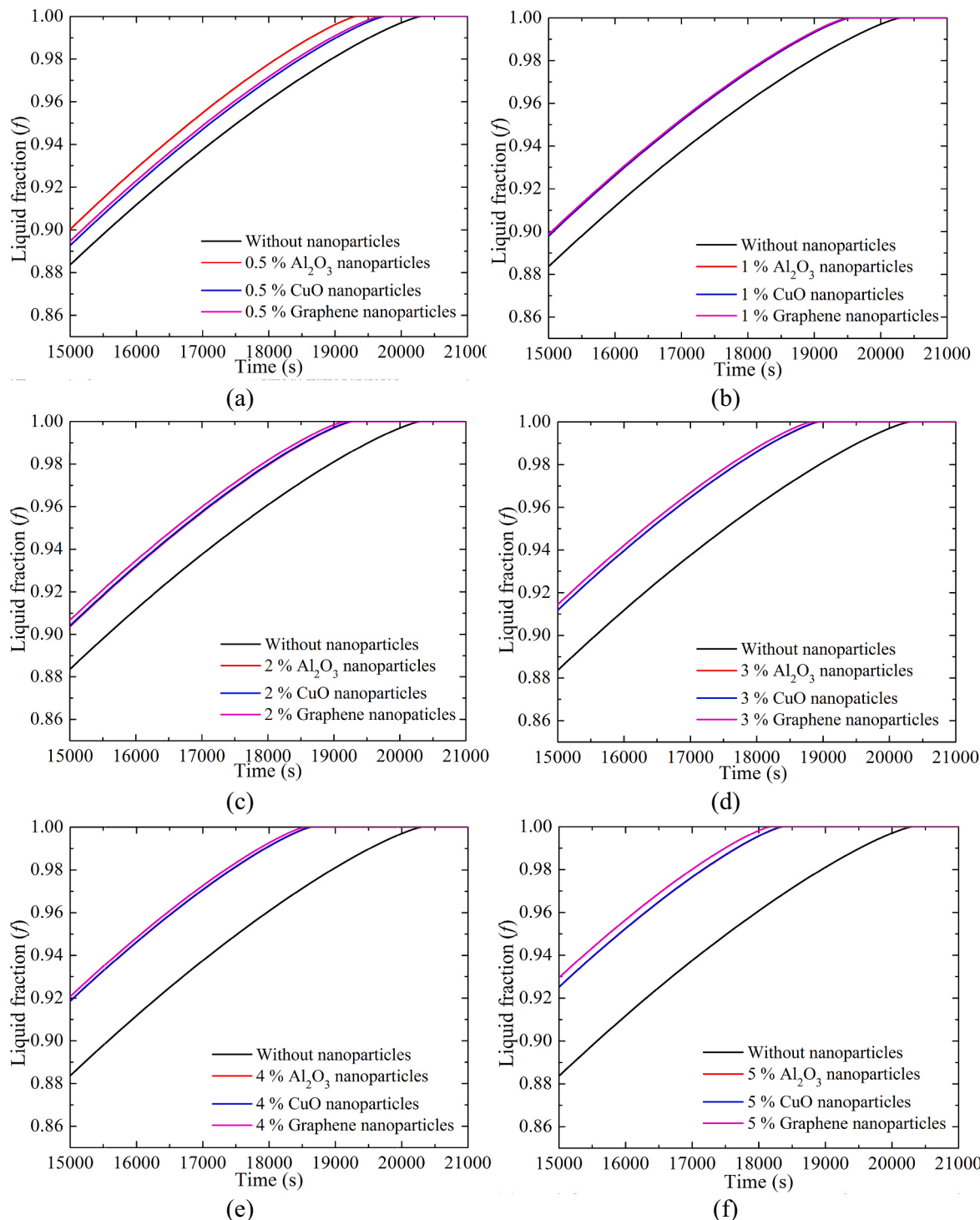


Fig. 10. Temporal evolution of liquid fraction with (a) $\varphi = 0.5\%$ and (b) $\varphi = 1\%$, (c) $\varphi = 2\%$, (d) $\varphi = 3\%$, (e) $\varphi = 4\%$, and (f) $\varphi = 5\%$ of Al_2O_3 , CuO and Graphene nanoparticles with its enlarged view when $\theta = 0^\circ$, $\Theta = 343\text{ K}$.

conductivity (5300 W/mK) than the two other metal oxide nanoparticles CuO (76.5 W/mK) and Al_2O_3 (46 W/mK). In the context of specific heat Al_2O_3 has the highest value (800 J/kg.K) compared to CuO (532.53 J/kg.K) and Graphene (700 J/kg.K) nanoparticles. Initially, with $\varphi = 0.5\%$ volume fraction, it can be noted that the total melting time is less for Al_2O_3 than for CuO and Graphene. It is due to the change in overall specific heat, density, latent heat of fusion, viscosity, and thermal conductivity. The performance is totally different when total melting time is considered because of their higher density and lower specific heat. On

the other hand, the system will experience an unpredictable trend in the melting process if the benefits of increasing thermal conductivity of NePCM are not surpassed by the drawbacks of decreasing specific heat and increasing viscosity and density. As the density of Al_2O_3 nanoparticles increases by 0.5 % but not as much as CuO and the specific heat of Al_2O_3 decreases but as CuO , because Al_2O_3 nanoparticles have the highest specific heat among them and density is close to Graphene and almost half of the CuO nanoparticles. Thus the 0.5 % Al_2O_3 nanoparticle shows the highest average melting rate. As the proportion of

nanoparticles within the volume rises, the overall density for NePCM increases, specific heat decreases, thermal conductivity increases, viscosity rises, and latent heat diminishes. Thus, As the proportion of volume fraction grows from $\varphi = 0.5\%$ to 1% the thermal conductivity of Graphene nanoparticles dominates as it has the highest thermal conductivity which is about >100 multiple of Al_2O_3 and about 70 multiple of CuO nanoparticles thermal conductivity. This trend continues up to a volume fraction of $\varphi = 3\%$. An almost consistent scenario is found for NePCM containing Al_2O_3 and CuO at concentrations ranging from $\varphi = 1\%$ to 3% , meaning that their presence or absence does slightly influence the PCM melting process. The procedure outlined for NePCMs having the metal oxide nanoparticles Al_2O_3 and CuO does not significantly improve NePCMs having carbon-based Graphene nanomaterials, as seen in Figs. 10(b), (c), and (d). Graphene can have a beneficial effect on the PCM melting process because of its exceptionally high heat conductivity and low density in comparison to the other metal oxides. The increase in the liquid percentage is evident as Graphene nanoparticle concentrations rise, as seen in Figs. 10(a) to (d). These nanomaterials have a lower density and a large heat capacity because of the structure of carbon of Graphene, which is an excellent benefit for the storage of thermal energy devices. For volume fractions of $\varphi = 4\%$ and 5% , it can be seen that the increment in volume fraction has a positive effect on average melting speed, but the different nanoparticles do affect the total melting as the total melting time is the same for all the nanoparticles for 4% volume fraction and two nanoparticles (CuO and Al_2O_3) for $\varphi = 5\%$ volume fraction, as shown in Fig. 10(e) and (f).

In this section, the influence of nanoparticle concentration on the melting process and energy storage efficiency of NePCMs can be explained by several key physical phenomena. As the concentration of nanoparticles increases, the thermal conductivity of the NePCM also increases due to the superior heat transfer properties of the nanoparticles. This results in faster heat distribution throughout the material, promoting quicker melting and improved energy storage rates. However, as the concentration rises, the viscosity of the NePCM also increases, which can delay the flow of liquid PCM during the melting process, slowing down natural convection and limiting heat transfer by fluid movement. Despite this, the enhanced thermal conductivity generally offsets the viscosity increase, allowing the overall melting rate to improve, especially at lower nanoparticle concentrations (from $\varphi = 0.5\text{--}3\%$).

The reduced latent heat of the PCM when nanoparticles are added is another important phenomenon. Nanoparticles disrupt the molecular structure of the PCM, lowering the energy required for phase transitions from solid to liquid. This effect further accelerates the melting process, contributing to the faster energy storage observed at higher nanoparticle concentrations. However, at very high concentrations (above $\varphi = 3\text{--}5\%$), the benefits from increased thermal conductivity are counterbalanced by the adverse effects of increased viscosity and reduced latent heat, leading to diminishing returns. These phenomena emphasize the importance of balancing nanoparticle concentration to optimize melting performance and energy storage efficiency in NePCMs.

4.3. Effect of inclination angle on thermal performance

In this section, 3% Graphene nanoparticles are considered for extending the further enhancement in the thermal performance of the PCM unit. Numerous studies have indicated that incorporating nanoparticles at this concentration into PCMs yields optimal results without any agglomeration or sedimentation of nanoparticles [2,35]. Beyond this threshold value, there is a notable occurrence of nanoparticle coagulation and sedimentation, significantly compromising the performance of the material. The present findings underscore this trend, revealing that escalating nanoparticle concentrations lead to viscosity dominating over other crucial thermal properties in the NePCM system. Fig. 11 illustrates the liquid fraction contours for different time frames with different inclination angles (θ). The effect of rectangular cavity

inclination on the PCM can have significant implications on the movement of heat and fluids inside the enclosure. Inclination, or the angle at which the cavity is positioned with respect to the horizontal plane, influences several key aspects of the thermal behavior and performance of the system. One effect is natural convection; inclination alters the natural convection patterns within the cavity. As the cavity is tilted, buoyancy-driven flow patterns change, affecting the circulation of the PCM and heat transfer rates. The direction and intensity of convection currents are modified, impacting the distribution of temperature gradients and the overall heat transfer process. Thus, as the angle of inclination rises, the overall duration of melting decreases but the volume fraction for 3% Graphene nanoparticles has very little impact on melting speed. At first 30 min the melting rate is high then the next 30 min and so on. The reason for conduction dominance lies in the proximity of the top heated wall to the solid-liquid interface of the PCM. The contour of the liquid fraction shows for 30 min , at 0° inclination many small convection shells were generated with clockwise and anti-clockwise directions. The same can be seen for the volume fraction of 3% Graphene. As inclination increases from 0° to 15° only one concentric convection shell is generated and the mushy zone is decreased. That means the interaction space between the completely melted liquid and the solid is less so the heat transfer rate will be higher. This phenomenon continues up to $\theta = 60^\circ$ inclination. At 90 min time frame for 0° inclination the small convection shells merge and create a bunch of larger convection shells than previous. The same can be seen in the 3% volume fraction of Graphene nanoparticles. It is clearly visible that as the inclination increases the convection shell enlarges and bounces back from the top layer of that enclose and pushes down the solid-liquid mushy zone interface. Thus, as the inclination increases the rate of melting increases. At the time frame of 150 min , a new stack of streamline produces for $\theta = 0^\circ$ inclination for both pure PCM and $\varphi = 3\%$ volume fraction of Graphene nanoparticles. When the inclination increases, a curvature of the liquid fraction line can be seen at the bottom corner of the mushy zone. As the inclination increases to 30° , a new anti-directional smaller convection shell has been generated under the big convection shell. As the inclination increases to 45° and 60° , the anti-directional convection shell collapses and merges with the existing bigger convection shell on the top. One other notable thing is that as the inclination increases the center of the concentric convection shell goes to the bottom side which is due to the bouncy effect. It has been determined that natural convection accelerates promptly following the onset of melting, evident from a vigorous fluctuation in the local Nusselt number and a sharp increase in the temperature of the liquid.

The phase change behavior also changes as the orientation of the cavity alters. As the cavity is inclined, gravitational forces affect the movement of the liquid-solid interface during melting or solidification processes. This leads to non-uniform phase change characteristics and variations in the temporal and spatial distribution of the phase change front. Inclination also affects the distribution of heat within the cavity. As the cavity is tilted, the spatial distribution of temperature gradients changes, leading to uneven heating or cooling of different regions within the cavity. This can impact thermal stratification, temperature homogeneity, and overall thermal performance. Depending on the orientation and geometry of the cavity, inclination enhances or hinders heat transfer rates. Optimally inclined cavities promote better mixing and circulation of the PCM, leading to improved heat transfer efficiency. Conversely, unfavorable inclinations create stagnant regions or flow separation zones, reducing heat transfer effectiveness. Inclination also influences the stability of fluid flow within the cavity. Certain inclinations induce flow instabilities, such as flow separation, vortex shedding, or boundary layer separation, which disrupt the heat transfer processes and affect system performance. Thus, the effect of inclination on a rectangular cavity with a top heated wall filled with PCM is a complex interplay of fluid dynamics, heat transfer phenomena, and phase change behavior.

The investigation revealed distinct behaviors in the liquid portion of the PCM depending on its location within the container. The upper part

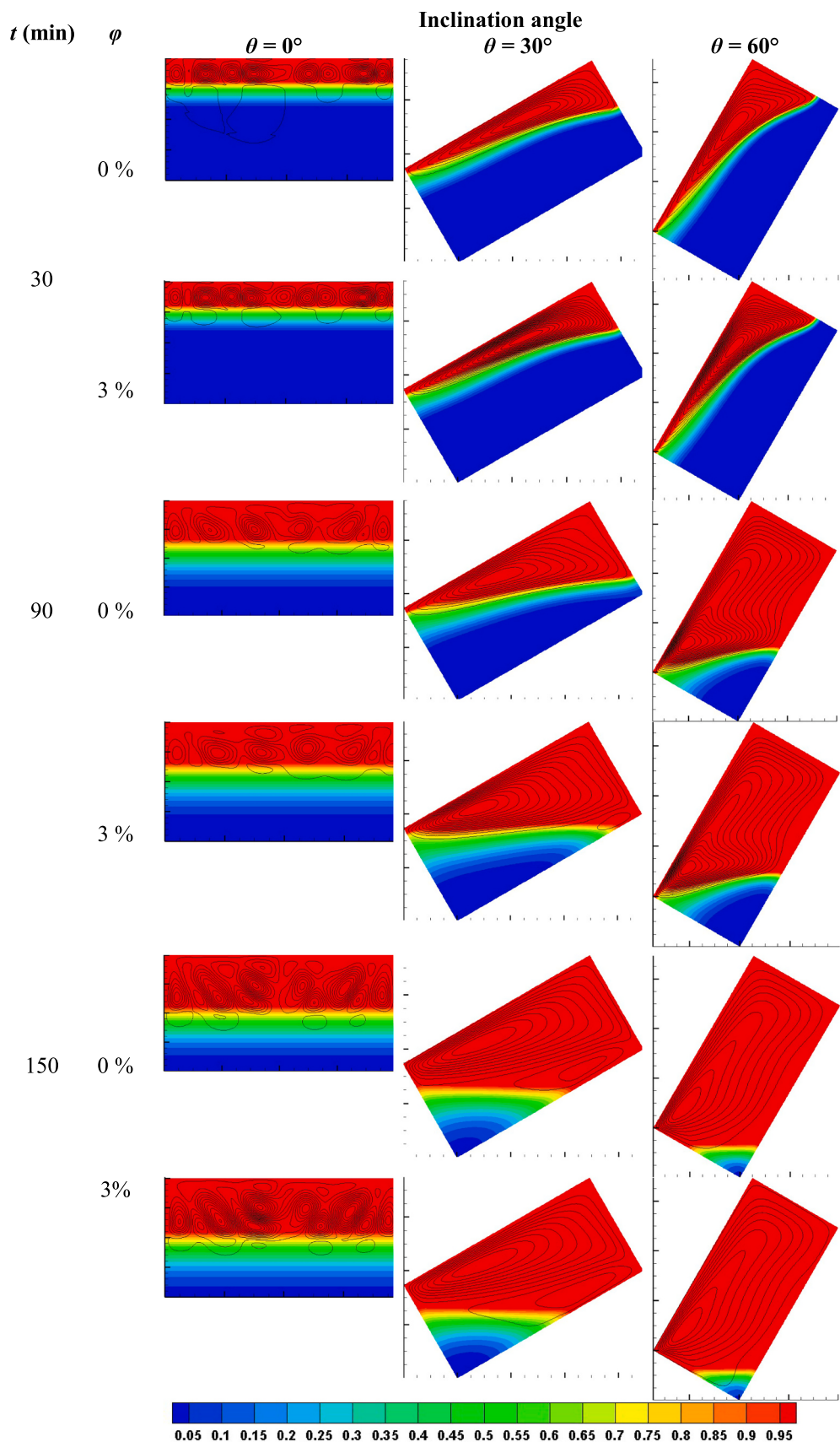


Fig. 11. Liquid fraction contours for best nanoparticle concentration ($\varphi = 0$ and 3 %) with different inclination angles (θ) varying time steps when $\Theta = 343$ K.

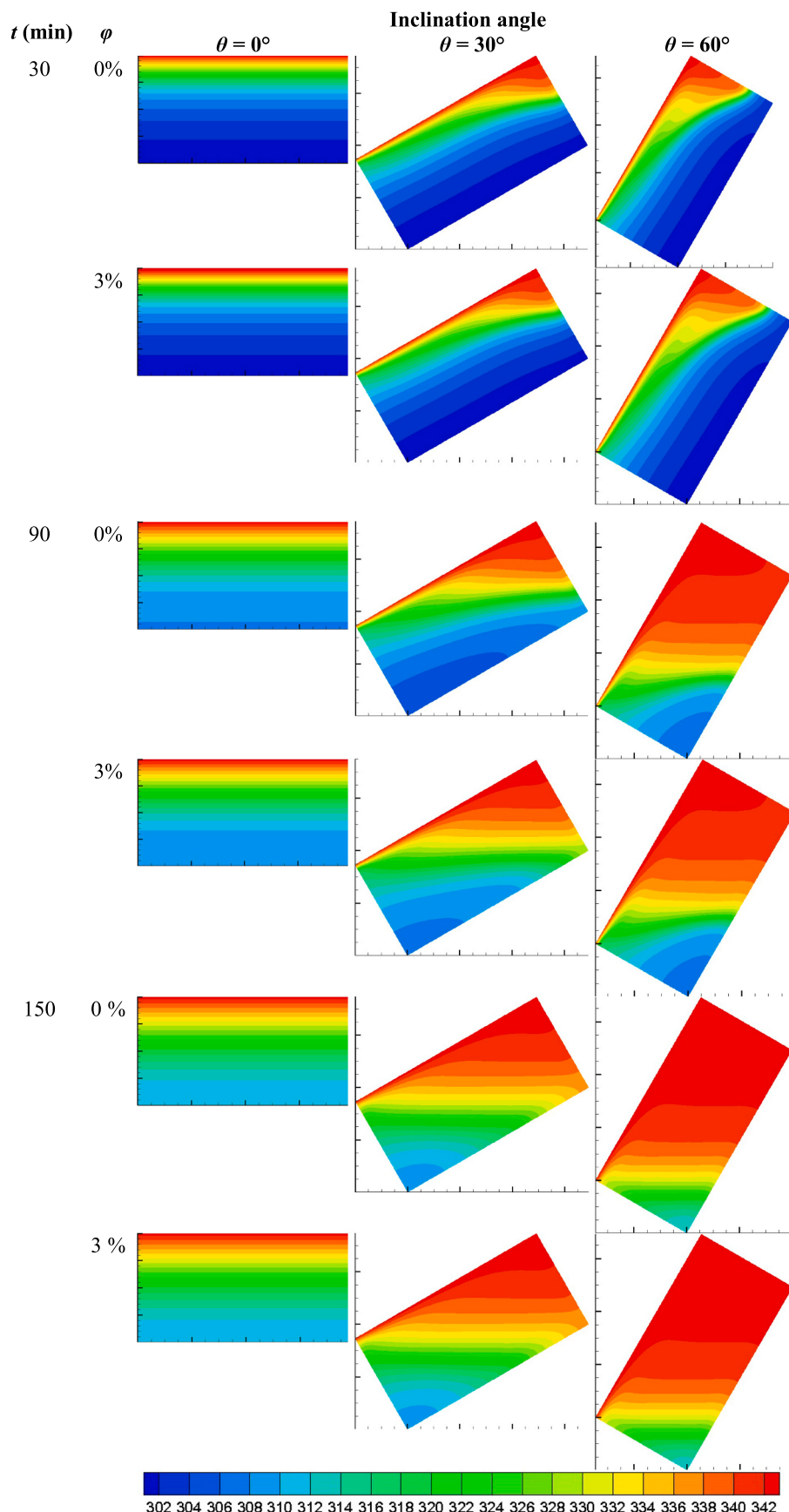


Fig. 12. Temperature contours for best nanoparticle concentration ($\varphi = 0$ and 3 %) with different inclination angles (θ) varying time steps when $\Theta = 343$ K.

consistently showed expansion compared to the lower section, resulting in a curved solid-liquid boundary, except when the container was completely level. As the tilt angle decreased, the extent of curvature reduced. Conversely, the lower part displayed a nearly linear boundary, except when the container was completely level, where it became more pronounced over time. This discrepancy was mainly due to a recirculation phenomenon caused by a temperature gradient. The heat circulation pattern induced by the temperature difference between the hot and cold sides led to a concentration of higher-temperature liquid PCM at the upper region, accelerating melting compared to the lower part. Consequently, a slightly curved boundary formed at the upper side, while at a $\theta = 0^\circ$, the boundary remained straight due to restricted liquid PCM movement. This indicates that increasing the tilt angle from 0° to 60° decreases the total melting time, primarily due to heightened convection heat transfer within the PCM.

Fig. 12 shows the temperature contours for various angles of cavity inclination (θ) and 3 % volume fractions (φ) for Graphene nanoparticles for different time frames at $t = 30, 90$, and 150 min. The contour reveals a notable temperature discrepancy between the upper and lower sections of the container. This variance stems from the fact that the top wall, serving as the primary heat source, induces conduction directly over the upper region. This phenomenon is particularly evident at a tilt angle of 0° . Beyond this angle, the upward migration of melted PCM near the heat source occurs due to a density shift caused by temperature elevation, with convection dominating heat transfer within the container due to the low thermal conductivity of PCM. This stratification becomes more pronounced, especially in cases with minor temperature differentials. Across all tilt angles, areas closest to the heated wall initially exhibit the highest temperatures due to conductive heat transfer. Subsequent columns register lower temperatures due to the limited thermal conductivity of the PCM. The temperature distribution varies significantly for different inclination angles.

When the cavity is horizontal ($\theta = 0^\circ$), the temperature distribution extends downward due to the temperature gradient caused by the top position of the heated wall. As the procedure advances and the solid material at the upper portion of the shell begins to liquefy, the melting process systematically progresses, starting from the lower layers of the shell. Increasing the inclination angle to $\theta = 15^\circ, 30^\circ, 45^\circ$, and 60° results in a similar temperature distribution pattern as at $\theta = 0^\circ$, but with higher temperatures reflecting the increased angle, as indicated in **Table 4**. **Table 4** introduces the average temperature of PCM and NePCM at 90 min. As the results show with the increasing the 3 % Graphene nanoparticles average temperature slightly increases but as the inclination angle increases the average temperature of PCM or NePCM increases drastically. An increase in the volume fraction of nanoparticles enhances the segment of thermal energy related to various angles of inclination, thus accelerating the melting rate. Concurrently increasing the inclination angle and nanoparticle volume fractions elevating the temperature of the PCM and NePCM enhances the heat transfer rate and accelerates the melting process. The temperature contours on different time frames and inclination angles in a rectangular cavity with a top heated wall filled with PCM is a complex phenomenon involving fluid dynamics, heat transfer, and phase change processes.

Fig. 11 depicts the relationship between liquid fraction and time across various inclination angles, focusing on the scenario involving pure PCM and $\varphi = 3\%$ of Graphene-mixed NePCM. As previously mentioned, elevating the inclination angle leads to a larger area

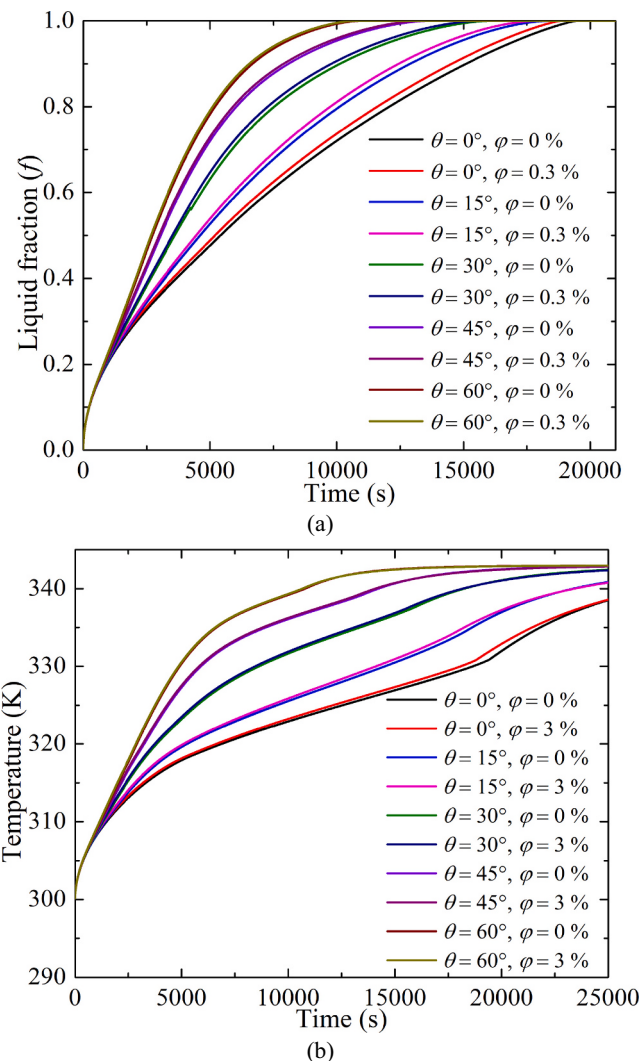


Fig. 13. (a) Liquid fraction (b) Average temperature of Graphene mixed NePCM with respect to time with increasing inclination angle (θ), nanoparticle concentration (φ) when $\Theta = 343$ K.

experiencing natural convection, thereby amplifying its effects. Thus, in turn, reduces the overall melting duration of the PCM. One other notable thing is that as the inclination increases the difference between the melting time and liquid fraction decreases and eventually at the angle of 60° the liquid fraction curve for both the PCM and NePCM merges with each other. **Fig. 13(a)** and (b) show the liquid fraction and average temperature change within the entire PCM-filled cavity throughout the melting process for different inclination angles. Generally, the liquid fraction increases steadily over time, approaching 1.0, indicating that the system moves towards complete liquid saturation as time progresses. Higher values of θ result in a faster rate of liquid fraction increase, with curves for $\theta = 60^\circ$ reaching higher liquid fractions more quickly than those for lower angles, such as $\theta = 0^\circ$. Similarly, the percentage parameter φ also influences the rate of change, as curves with $\varphi = 3\%$ exhibit a faster rise in liquid fraction compared to those with $\varphi = 0\%$. The overall trend demonstrates that both the angle and the percentage play critical roles in accelerating the transition of the system to a higher liquid fraction, with noticeable differences between the curves based on these variables. The time required for the liquid fraction to reach near-saturation ranges from 5000 to 20,000 s, depending on the specific conditions of θ and φ . For every inclination angle first fast heating occurs due to the conduction which occurs for sensible heating, after that a stagnant average temperature curve has been seen which indicates the

Table 4

The average temperature of PCM and Graphene nanoparticles mixed NePCM at $t = 90$ min, when $\Theta = 343$ K.

| Nanoparticle concentration (φ) | Average temperature (K) | | | | |
|--|-------------------------|---------------------|---------------------|---------------------|---------------------|
| | $\theta = 0^\circ$ | $\theta = 15^\circ$ | $\theta = 30^\circ$ | $\theta = 45^\circ$ | $\theta = 60^\circ$ |
| 0 % | 318.395 | 320.210 | 324.207 | 328.581 | 331.764 |
| 3 % | 318.634 | 320.469 | 324.494 | 328.805 | 331.942 |

melting process thus latent heating. A sudden increase can be seen which shows the sensible heating after the completion of the melting process and the overall temperature reaches the heated wall temperature and a steady state temperature occurs.

The variation of average temperature with respect to time, with different inclination angles of the enclosure featuring a heated upper surface containing PCM, is a critical aspect of understanding the thermal behavior and performance of the system. The inclination angle of the

cavity significantly affects natural convection patterns within the PCM. As the cavity is tilted, buoyancy-driven flow patterns change, altering the circulation of the PCM and affecting heat transfer rates. This change in flow dynamics leads to variations in the average temperature within the cavity over time. The inclination angle also impacts the phase change behavior of the PCM. Gravitational forces acting on the PCM influence the movement of the liquid-solid interface during melting or solidification processes. This has resulted in variations in the rate of heat

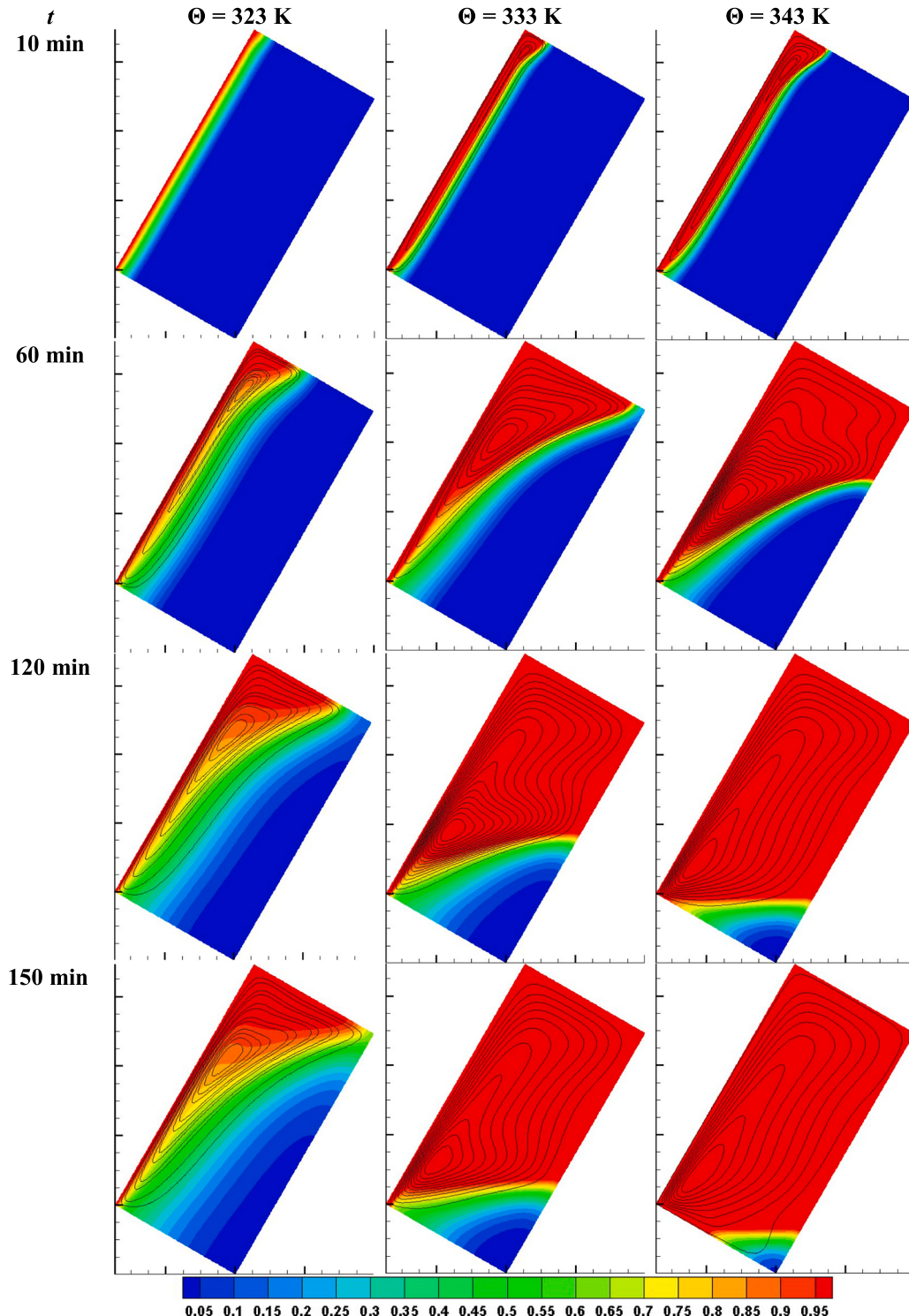


Fig. 14. Liquid fraction contour with respect to different time frames for the different heating wall temperatures (Θ) for the Graphene nanoparticles mixed NePCM when $\varphi = 3\%$ and $\theta = 60^\circ$.

absorption or release, affecting the temporal evolution of the average temperature within the cavity. Different inclination angles result in uneven distribution of heat within the cavity. As the cavity is tilted, the spatial distribution of temperature gradients changes, leading to non-uniform heating or cooling of different regions within the cavity. This influences the average temperature profile over time, with certain inclination angles promoting more uniform temperature distributions than others. The efficiency of heat transfer within the cavity can be influenced by the inclination angle. Optimal inclination angles enhance heat transfer rates by promoting better mixing and circulation of the PCM, resulting in more efficient thermal energy storage or release. Changes in inclination angle also affect transient heat transfer phenomena within the cavity. Transient responses, such as the time taken for the PCM to reach equilibrium temperature or the duration of phase change processes, vary with different inclination angles. Understanding these transient effects is crucial for predicting the dynamic behavior of the system over time.

The physical phenomenon underlying the observed trends in the graph of Fig. 13 (a) likely relates to heat transfer and phase change processes. The angle θ represents the inclination of a surface or the orientation of a heat source, with higher angles improving the rate of heat transfer due to enhanced convection or a more favorable orientation for heat diffusion. This explains why the liquid fraction increases more rapidly for larger θ values. Similarly, the parameter φ likely represents a factor such as the presence of impurities or enhanced thermal conductivity, which accelerates the rate of phase change. Systems with a higher φ show faster liquid formation, as indicated by the curves with $\varphi = 3\%$ rising more quickly than those with $\varphi = 0\%$. The interplay between θ and φ modifies the heat transfer efficiency, thereby influencing how quickly the system transitions from a solid to a liquid state.

The physical phenomenon governing the effect of inclination angle on the thermal performance of NePCMs involves a shift in the dominant heat transfer mechanism from conduction to convection as the angle increases. At lower inclination angles, heat transfer is primarily driven by conduction, especially near the heated wall where a thin layer of liquid PCM forms and propagates. As the inclination angle increases, natural convection becomes more prominent due to buoyancy effects, which are enhanced by the greater temperature gradient in the liquid PCM. This buoyancy-driven flow leads to increased fluid motion, promoting more uniform heat distribution and faster melting. The interaction between conduction and convection in the NePCM system is further influenced by the type and concentration of nanoparticles, with

higher thermal conductivity materials (such as Graphene) facilitating more efficient convective heat transfer. As a result, the melting rate and overall thermal performance improve with increased inclination angles, with the optimal performance typically occurring at angles around $\theta = 60^\circ$, where convection dominates and enhances the overall energy storage efficiency.

4.4. Effect of temperature on thermal performance

The thermal performance of PCMs is significantly influenced by the operating temperature. The behavior of the PCM at three distinct temperatures $\Theta = 323\text{ K}$, 333 K , and 343 K is shown in Figs. 14 and 15 for the Graphene-mixed NePCM when $\varphi = 3\%$ and $\theta = 60^\circ$. $\varphi = 3\%$ Graphene nanoparticles are evaluated for their potential to further enhance the thermal performance of the PCM unit. Exceeding this concentration threshold results in significant nanoparticle coagulation and sedimentation, which substantially degrades the performance of the material. The current findings highlight this pattern, demonstrating that increasing nanoparticle concentrations lead to viscosity becoming the dominant factor over other essential thermal properties in the NePCM system. These temperatures are chosen to understand how different levels above the liquidus temperature impact the melting rate of the PCM, energy storage capacity, and overall efficiency. By investigating these parameters, the usage of PCM in thermal energy storage applications is optimized ensuring maximum efficiency and reliability across various temperature ranges.

At an initial stage ($t = 0\text{ min}$), the PCM begins to melt as $\Theta = 323\text{ K}$ is just above the liquidus temperature of 322 K , though it starts in a solid state. During early melting ($t = 10\text{ min}$), the liquid fraction increases near the heat source as the temperature reaches 323 K , forming a temperature gradient with the highest temperatures close to the heat source. In the intermediate melting stage ($t = 60\text{ min}$), a portion of the PCM transitions to liquid, with the liquid fraction progressively increasing, and the temperature contours expanding outward from the heat source, showing some part of the PCM nearing 323 K . By the advanced melting stage ($t = 120$, and 150 min), even half of the PCM is not liquid, with more than half of the part remaining solid, farthest from the heat source, and the temperature is nearly uniform at 323 K throughout some of the part of PCM which is visible in the Fig. 14. Finally, in the complete melting stage, which is $>420\text{ min}$ as shown in Fig. 15, the entire PCM has melted, and the temperature is uniformly 323 K across the PCM.

At a temperature of $\Theta = 333\text{ K}$, the PCM initially starts as a solid but will melt faster compared to $\Theta = 323\text{ K}$ since 333 K is higher above the liquidus temperature. During the early melting stage ($t = 10\text{ min}$), the melting process begins more rapidly, with a swift increase in the liquid fraction near the heat source and a steeper temperature gradient as the PCM quickly reaches $\Theta = 333\text{ K}$. As shown in Fig. 14, the intermediate melting stage ($t = 60\text{ min}$), a larger volume of PCM is liquid compared to the same stage at $\Theta = 323\text{ K}$, with temperature contours spreading more rapidly and covering a greater area at $\Theta = 333\text{ K}$. By the advanced melting stage ($t = 120$, and 150 min), the majority of the PCM is in a liquid state sooner, and the temperature becomes nearly uniform at 333 K across most of the PCM. Finally, in complete melting, the PCM achieves complete melting faster, resulting in a uniform temperature of 333 K throughout.

At a temperature of $\Theta = 343\text{ K}$, the PCM initially starts solid but melts even faster than at 333 K due to the higher temperature. In the early melting stage ($t = 10\text{ min}$), there is a very rapid increase in the liquid fraction near the heat source, accompanied by a steeper temperature gradient with a quick rise to 343 K . During the intermediate melting stage ($t = 60\text{ min}$), a much larger portion of the PCM is liquid compared to lower temperatures, with most of the PCM quickly approaching 343 K . In the advanced melting stage ($t = 150\text{ min}$), the PCM is almost entirely liquid, and the temperature is nearly uniform at 343 K throughout. Finally, in the complete melting stage, the PCM experiences the fastest complete melting, achieving a uniform 343 K temperature

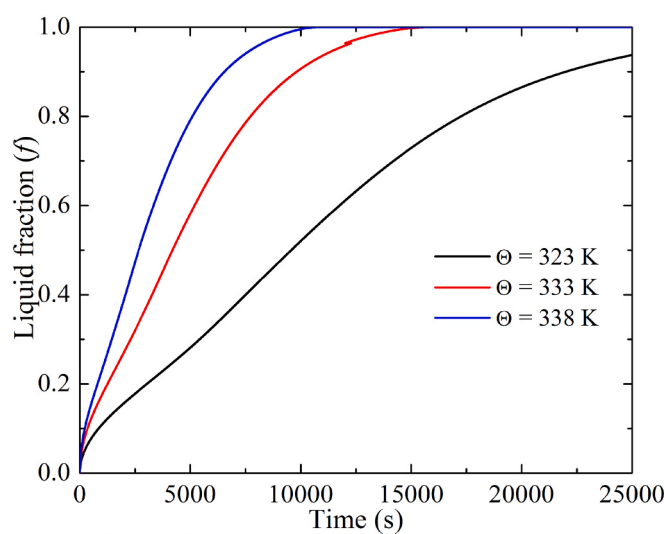


Fig. 15. Liquid fraction with respect to time with various heating wall temperatures (Θ) for the Graphene nanoparticles mixed NePCM when $\varphi = 3\%$ and $\theta = 60^\circ$.

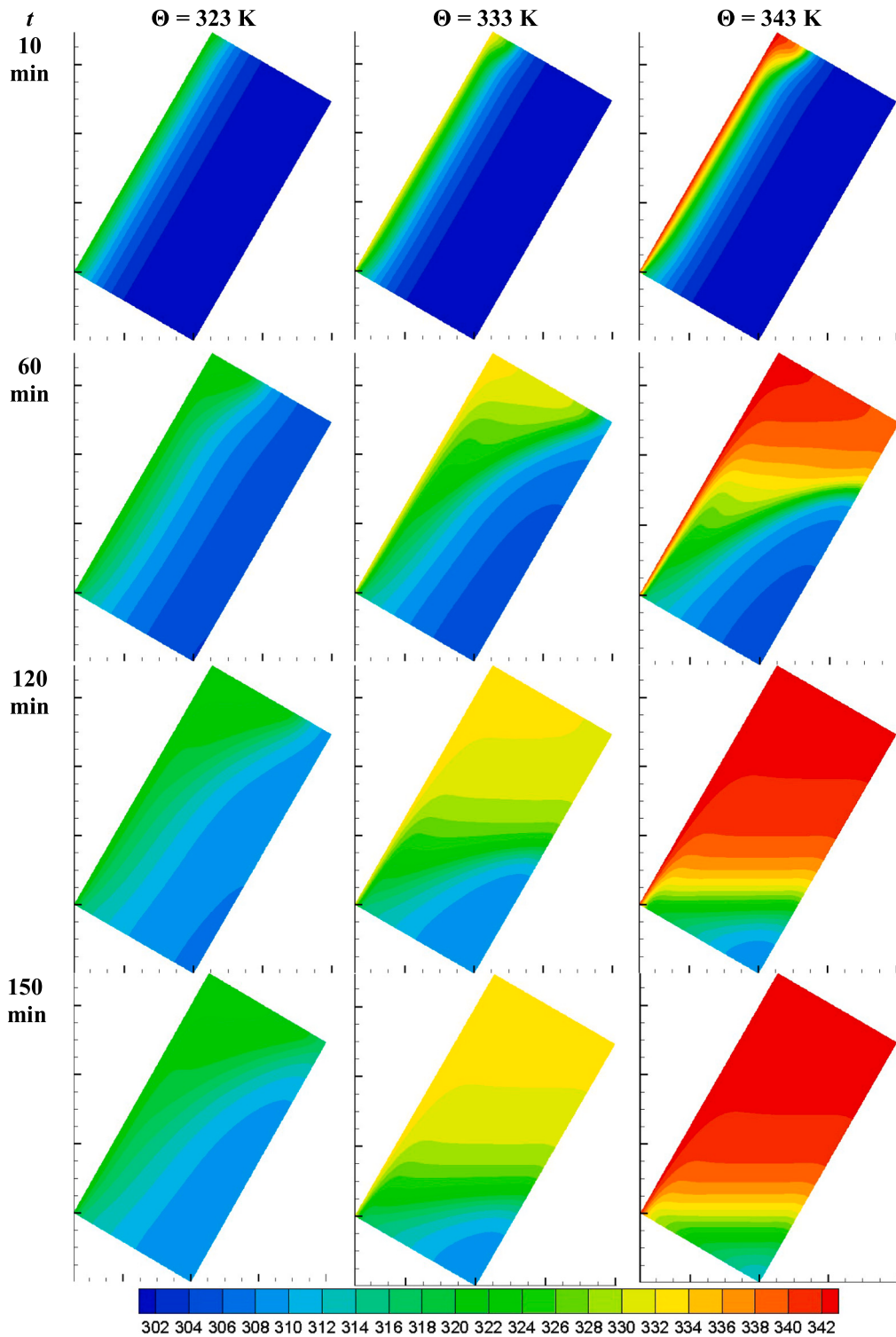


Fig. 16. Average temperature contour with respect to different time frames with heating wall temperature (Θ) for the Graphene nanoparticles mixed NePCM when $\varphi = 3\%$ and $\theta = 60^\circ$.

across the entire material.

Fig. 15 shows higher temperatures lead to faster melting of the PCM, with $\Theta = 333 \text{ K}$ and 343 K causing more rapid phase transitions compared to 323 K due to the greater temperature difference from the liquidus point. This increased temperature difference also enhances the heat transfer rate by creating steeper temperature gradients. Furthermore, as the temperature rises, the PCM achieves a uniform temperature distribution more quickly after melting, indicating more efficient

thermal performance.

For each temperature ($\Theta = 323 \text{ K}$, 333 K , and 343 K), we plot the liquid fraction versus time and the temperature contours to visualize the thermal performance shown in Figs. 15 and 16 respectively. At $\Theta = 323 \text{ K}$, there is a gradual increase in the liquid fraction, indicating a slower melting process. The temperature contours show a gradual spreading of the 323 K isotherms throughout the PCM. At $\Theta = 333 \text{ K}$, the liquid fraction increases more quickly, reflecting a faster melting rate, with the

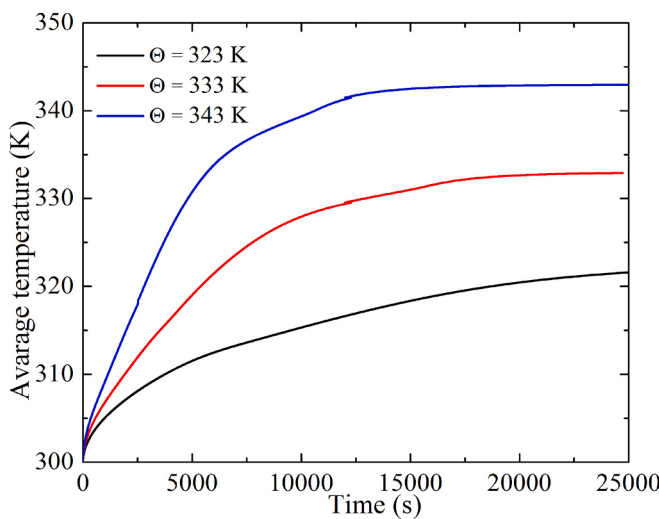


Fig. 17. Average temperature with respect to time with various heating wall temperatures (Θ) for the Graphene nanoparticles mixed NePCM when $\varphi = 3\%$ and $\theta = 60^\circ$.

temperature contours spreading more rapidly. At $\Theta = 343$ K, the liquid fraction reaches its maximum at the fastest rate, demonstrating the quickest melting process, with the temperature contours spreading rapidly across the PCM. This visual representation highlights how higher temperatures accelerate both the melting process and the thermal distribution within the PCM.

Fig. 17 shows how quickly the PCM transitions from solid to liquid at different temperatures and how the temperature distribution evolves over time. The effect of temperature on thermal performance is primarily governed by the physical phenomena of heat transfer, phase change dynamics, and thermal conductivity. As the temperature of the heated wall increases, the rate of heat transfer to the PCM also increases, resulting in a faster transition from solid to liquid. This is because higher wall temperatures provide a larger temperature gradient, which drives heat conduction more effectively, leading to quicker melting. Additionally, as the PCM absorbs heat and reaches its melting point, the latent heat of fusion facilitates the phase transition without raising the temperature of the material, ensuring a near-isothermal process during the phase change. For NePCMs, the inclusion of nanoparticles further amplifies the thermal performance due to the increased thermal conductivity. The higher the temperature of the heated wall, the more efficiently these nanoparticles can distribute heat throughout the PCM, reducing melting times and improving energy storage capacity. However, if the temperature increases beyond optimal levels, viscosity and other fluid properties may negatively impact the natural convection process, slowing down the overall performance. Therefore, the relationship between temperature and thermal performance is a balance between enhanced heat transfer and potential changes in fluid dynamics.

4.5. Comparative performance enhancement

4.5.1. Average melting speed

The average melting speed (g/min) is influenced by both the concentration of nanoparticles and the inclination angle. Higher nanoparticle concentrations generally lead to an increased melting speed due to the enhanced thermal conductivity, which improves heat transfer and accelerates the melting process. Additionally, the inclination angle affects the natural convection currents within the PCM. Steeper angles can enhance these currents, further increasing the melting speed. Therefore, both higher nanoparticle concentrations and optimal inclination angles are crucial for maximizing the melting speed and overall performance of NePCMs in thermal energy storage applications.

Upon introducing nanoparticles, such as $\varphi = 0.5\%$ volume fraction of Al_2O_3 , remarkable improvements in thermal performance are observed. The melting speed reaches its peak at 8.759 g/min. This represents a notable enhancement over the performance of other additives, including Graphene (8.587 g/min) and CuO (8.556 g/min), as depicted in detail in Table 5. As the investigation progresses, variations in thermal performance are noted with changes in the volume fraction of Al_2O_3 . Specifically, when the volume fraction increases to $\varphi = 1\%$, a slight decrement is observed in both the melting speed (8.648 Kg/min). This contrasts with the performance of CuO, which experiences an up-tick in melting speed (8.627 g/min), while Graphene nanoparticles demonstrate a steady increase (8.666 g/min).

It is notable that Graphene nanoparticles emerge as a consistent frontrunner across volume fractions ranging from $\varphi = 1\%$ to 5 %. Its melting speeds range from 8.823 to 9.299 g/min. This remarkable consistency underscores the significant potential of Graphene-based PCM composites as highly efficient solutions for thermal energy storage applications in diverse settings.

The inclination angle significantly influences the gravitational force exerted on the PCM within the cavity. As the inclination angle increases, the gravitational force component parallel to the heated wall also increases, resulting in variations in the downward movement of the melted PCM and subsequently affecting the overall melting rate. This inclination further influences the formation of thermal stratification within the cavity during the melting process, as illustrated in Table 6. The average melting speed and energy storage rate are notably affected by the inclination angle, as shown in Table 6. For $\theta = 15^\circ$ inclination, the average melting speeds for pure PCM and NePCM are 9.194 g/min and 9.450 g/min, respectively, whereas, for $\theta = 60^\circ$ inclination, these speeds increase to 15.472 g/min and 15.759 g/min, respectively, which is nearly double the speeds observed at a 0° inclination.

Temperature gradients along the height and width of the cavity vary

Table 6

Average melting speed (g/min) of PCM and Graphene nanoparticles mixed NePCM ($\varphi = 3\%$) for the different inclination angles ($\theta = 0^\circ, 15^\circ, 30^\circ, 45^\circ$, and 60°) when $\Theta = 343$ K.

| Nanoparticle concentrations | Average melting speed (g/min) | | | | |
|-----------------------------|-------------------------------|---------------------|---------------------|---------------------|---------------------|
| | $\theta = 0^\circ$ | $\theta = 15^\circ$ | $\theta = 30^\circ$ | $\theta = 45^\circ$ | $\theta = 60^\circ$ |
| $\varphi = 0\%$ | 8.323 | 9.194 | 10.578 | 12.469 | 15.472 |
| $\varphi = 3\%$ | 8.961 | 9.450 | 10.831 | 12.738 | 15.759 |

Table 5

Average melting speed of NePCM for three different nanoparticles with concentrations ($\varphi = 0\%$ to 5 %), when $\Theta = 343$ K and $\theta = 0^\circ$.

| Properties | Average melting speed (g/min) of NePCM | | | | | | |
|---|--|-------------------|-----------------|-----------------|-----------------|-----------------|-----------------|
| | $\varphi = 0\%$ | $\varphi = 0.5\%$ | $\varphi = 1\%$ | $\varphi = 2\%$ | $\varphi = 3\%$ | $\varphi = 4\%$ | $\varphi = 5\%$ |
| Pure PCM | 8.323 | — | — | — | — | — | — |
| PCM + Al_2O_3 nanoparticles | — | 8.759 | 8.648 | 8.788 | 8.927 | 9.065 | 9.204 |
| PCM + CuO nanoparticles | — | 8.556 | 8.627 | 8.777 | 8.931 | 9.071 | 9.209 |
| PCM + Graphene nanoparticles | — | 8.587 | 8.666 | 8.823 | 8.961 | 9.074 | 9.299 |

Table 7

Average melting speed (g/min) of pure PCM and Graphene nanoparticles mixed NePCM ($\varphi = 3\%$) for three different heated wall temperatures (Θ) when $\theta = 60^\circ$.

| Criteria | Average melting speed (g/min) | | |
|--|-------------------------------|-------------------------|-------------------------|
| | $\Theta = 323\text{ K}$ | $\Theta = 333\text{ K}$ | $\Theta = 343\text{ K}$ |
| PCM + Graphene nanoparticles ($\varphi = 3\%$) | 4.02 | 10.591 | 15.759 |

with the inclination angle, leading to differences in heat transfer rates and melting speeds across various regions. Additionally, the inclination angles modify the fluid flow patterns induced by natural convection within the PCM during melting. As the cavity tilts, the buoyancy-driven flow patterns change, affecting the circulation of the molten PCM and thereby influencing the melting speed. The inclination angle influences the orientation of the phase transition front, which separates the solid and liquid phases of the PCM. Differences in the average melting speed are a result of the impact of variations in the frontal orientation and propagation speed on the overall melting process. The average melting speed (g/min) of RT-45 with $\varphi = 3\%$ Graphene nanoparticles for three different heated walls $\Theta = 323\text{ K}$, 333 K , and 343 K are given in Table 7.

Optimally inclined cavities enhance the mixing and circulation of the PCM, promoting improved heat transfer efficiency and faster melting rates. The effect of inclination angle on the average melting speed in a rectangular cavity with a top heated wall filled with PCM involves a complex interplay of gravitational forces, fluid dynamics, thermal stratification, and heat transfer phenomena. The average melting speed of NePCMs is driven by increased thermal conductivity and reduced latent heat due to the addition of nanoparticles like Al_2O_3 , CuO , and Graphene nanoparticles. This enhances heat transfer and requires less energy for melting, accelerating the process. While higher nanoparticle concentrations can increase viscosity and slow convection, the overall effect is a faster melting speed, particularly at optimal nanoparticle concentrations and configurations that maximize heat transfer efficiency.

4.5.2. Energy storage rate

Similarly, the energy storage rate varies with the inclination angle and nanoparticle concentration, as shown in Tables 8 and 9. Higher angles result in an increased energy storage rate due to improved natural convection effects, which enhance heat transfer within the PCM. Additionally, higher nanoparticle concentrations further boost the energy storage rate by increasing thermal conductivity and facilitating more efficient heat absorption and distribution. This combined effect of inclination angle and nanoparticle concentration demonstrates the critical factors that influence the performance of NePCMs, underscoring the need for precise optimization to maximize energy storage efficiency in thermal energy storage systems.

Introducing nanoparticles, such as $\varphi = 0.5\%$ volume fraction of Al_2O_3 , leads to significant thermal performance improvements, achieving an energy storage rate of 1223.687 J/min. This rate exceeds that of other additives like Graphene (1199.741 J/min) and CuO (1195.366 J/min) nanoparticles, as detailed in Table 5. Performance variations occur with changes in the volume fraction of Al_2O_3 nanoparticles. When the fraction increases to 1%, a slight decrease in the energy storage rate to 1208.247 J/min is observed. In contrast, CuO shows an improvement at this volume fraction, reaching an energy

Table 9

Average energy storage rate (J/min) for pure PCM and Graphene nanoparticle concentrations ($\varphi = 3\%$) at different inclination angles ($\theta = 0^\circ, 15^\circ, 30^\circ, 45^\circ$, and 60°) when $\Theta = 343\text{ K}$.

| Nanoparticle concentrations (φ) | Average energy storage rate (J/min) | | | | |
|---|-------------------------------------|---------------------|---------------------|---------------------|---------------------|
| | $\theta = 0^\circ$ | $\theta = 15^\circ$ | $\theta = 30^\circ$ | $\theta = 45^\circ$ | $\theta = 60^\circ$ |
| 0 % | 1162.80 | 1284.416 | 1477.818 | 1741.971 | 2161.512 |
| 3 % | 1251.920 | 1320.191 | 1513.155 | 1779.531 | 2201.633 |

storage rate of 1205.316 J/min, while Graphene demonstrates a steady increase, reaching 1210.664 J/min as given in Table 8.

Graphene consistently shows superior performance across volume fractions ranging from $\varphi = 1\%$ to 5% , with energy storage rates from 1232.602 to 1299.191 J/min. This consistency underscores the significant potential of Graphene-based PCM composites as highly efficient solutions for thermal energy storage applications in various settings.

The angle at which a cavity is inclined plays a crucial role in determining the heat transfer mechanisms within a system that includes PCMs. When the cavity is angled, it changes the distribution of temperature gradients and the flow patterns of the PCM, thus influencing the energy storage rate. Different inclination angles can lead to variations in convective heat transfer and phase change behavior, affecting the overall rate of energy storage. The rate at which the PCM absorbs or releases thermal energy is particularly affected by the inclination angle. Some angles can improve the mixing and circulation of the PCM, enhancing heat transfer and storage capacity, while other angles may obstruct these processes and lower energy storage rates.

The inclination angle also influences the phase transition properties of the PCM. Gravitational forces acting on an inclined cavity alter the movement of the liquid-solid interface during melting or solidification, impacting the rate of energy storage and the progression of thermal energy within the system. For example, as shown in Table 9, the average energy storage rates for $\theta = 15^\circ$ inclination are 1284.416 J/min for pure PCM and 1320.191 J/min for NePCM. At a $\theta = 60^\circ$ inclination, these rates rise to 2161.512 J/min and 2201.633 J/min, respectively, nearly double the values at a 0° inclination.

The average energy storage rate (J/min) of RT-45 with 3% Graphene nanoparticles for three different heated walls $\Theta = 323\text{ K}$, 333 K , and 343 K are given in Table 10.

Determining the optimal inclination angle, which maximizes the energy storage rate, involves numerical simulations that take into account factors like fluid dynamics, heat transfer efficiency, and phase change kinetics. These simulations identify the specific inclination angle that offers the best performance for a given cavity and PCM combination. The energy storage rate in NePCMs is primarily driven by the improved thermal conductivity from nanoparticles like Al_2O_3 , CuO , and

Table 10

Average energy storage rate (J/min) of NePCM for three different heated wall temperature (Θ) when $\theta = 60^\circ$.

| Properties | Average energy storage rate (J/min) | | |
|--|-------------------------------------|-------------------------|-------------------------|
| | $\Theta = 323\text{ K}$ | $\Theta = 333\text{ K}$ | $\Theta = 343\text{ K}$ |
| PCM + Graphene nanoparticles ($\varphi = 3\%$) | 561.76 | 1479.67 | 2201.633 |

Table 8

Average energy storage rate (J/min) of NePCM for three different nanoparticles with concentrations ($\varphi = 0\%$ to 5%), when $\Theta = 343\text{ K}$ and $\theta = 0^\circ$.

| Criteria | Average energy storage rate (J/min) | | | | | | |
|---|-------------------------------------|----------|----------|----------|----------|----------|----------|
| | 0 % | 0.5 % | 1 % | 2 % | 3 % | 4 % | 5 % |
| Pure PCM | 1162.80 | — | — | — | — | — | — |
| PCM + Al_2O_3 nanoparticles | — | 1223.687 | 1208.247 | 1227.697 | 1247.127 | 1266.497 | 1285.885 |
| PCM + CuO nanoparticles | — | 1195.366 | 1205.316 | 1226.185 | 1247.685 | 1267.279 | 1286.586 |
| PCM + Graphene nanoparticles | — | 1199.741 | 1210.664 | 1232.602 | 1251.920 | 1267.755 | 1299.191 |

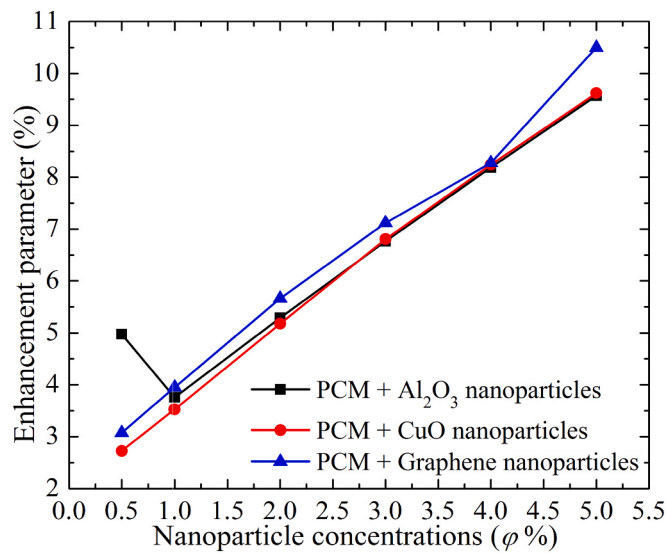


Fig. 18. Enhancement parameters for Al_2O_3 , CuO, and Graphene nanoparticles at various concentration of nanoparticles (φ) when $\Theta = 343$ K.

Graphene nanoparticles, which enable faster heat transfer and quicker melting. This accelerates the absorption of latent heat during the phase change, increasing the overall energy storage rate. While higher nanoparticle concentrations can raise viscosity and slow natural convection, the enhanced thermal conductivity generally outweighs these effects, leading to more efficient energy storage in NePCMs.

4.5.3. Enhancement parameters

The investigation of the enhancement parameters reveals intriguing dynamics across different volume fractions of Al_2O_3 , CuO, and Graphene nanoparticles, as showcased in Fig. 18. Initially, $\varphi = 0.5\%$ volume fraction of Al_2O_3 boasts the highest enhancement factor at an impressive 4.975 % when compared against the baseline of pure PCM. In this scenario, Graphene nanoparticles follows suit with a commendable enhancement factor of 3.076 %, while CuO trails closely behind at 2.724 %. However, as the volume fraction increases to $\varphi = 1\%$, it is observed that a nuanced shift in the enhancement parameter. The enhancement parameter for Al_2O_3 nanoparticles slightly recedes to 3.761 %, signifying a delicate interplay between volume fraction and enhancement parameter. Intriguingly, CuO nanoparticles experiences a contrasting trend, exhibiting a notable uptick to 3.527 %, indicative of its evolving role in the composite material. Yet, it is Graphene that steals the spotlight once again, showcasing its prowess with a remarkable enhancement of 3.953 % at the 1 % volume fraction. Even more intriguing is the fact that this pattern continues and even gets stronger with consecutive volume fractions. At $\varphi = 2\%$, 3% , 4% , and 5% volume fractions, the enhancement parameter for Graphene soared to staggering heights, reaching 5.662 %, 7.118 %, 8.278 %, and a remarkable 10.498 %, respectively.

This intricate progression highlights the unparalleled efficacy of Graphene in augmenting the properties of the composite material across a spectrum of volume fractions. The observed trends not only shed light on the performance of the material but also offer valuable insights into the optimization of composite formulations for enhanced functionality and performance in various applications. The examination of melting speed and total energy storage rate across various PCMs and their composites unveils intriguing insights into their thermal performance. Initially, the study begins by assessing the baseline performance of pure PCM, which exhibits a melting speed of 8.323 g/min and an energy storage rate of 1162.80 J/min. This establishes a reference point against which the enhancements achieved through the introduction of additives can be compared.

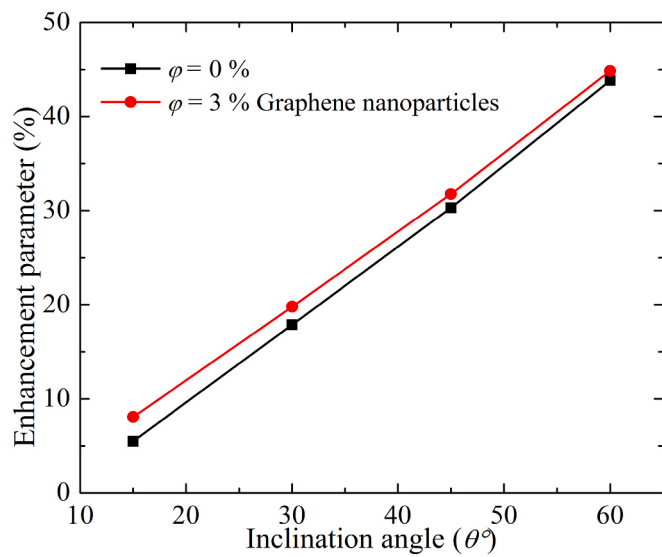


Fig. 19. Melting performance enhancement for different inclination angles (θ) of the cavity for the 3 % Graphene nanoparticles (φ) and pure PCM when $\Theta = 343$ K.

By raising the inclination angle starting from $\theta = 0^\circ$ to 15° , 30° , 45° and 60° the enhancement parameter increases to 5.492 %, 17.860 %, 30.316 % and 43.841 % respectively in the case of pure PCM and 8.053 %, 19.778 %, 31.787 % and 44.865 % respectively in case of NePCM with compare to the pure PCM with 0° inclination as shown in Fig. 19.

The results demonstrate a significant improvement in the melting rate and energy storage efficiency of NePCMs compared to pure PCMs, attributed to several contributing factors. First, the incorporation of nanoparticles like Al_2O_3 , CuO, and Graphene increases thermal conductivity, particularly Graphene with its high value of 5300 W/m·K, enabling more efficient heat transfer and faster melting. While higher nanoparticle concentrations also increase viscosity, which can impede natural convection, the boost in thermal conductivity generally outweighs this effect, leading to an overall improvement in melting rate. Additionally, the inclination angle plays a crucial role, with higher angles (especially at $\theta = 60^\circ$) enhancing natural convection due to stronger

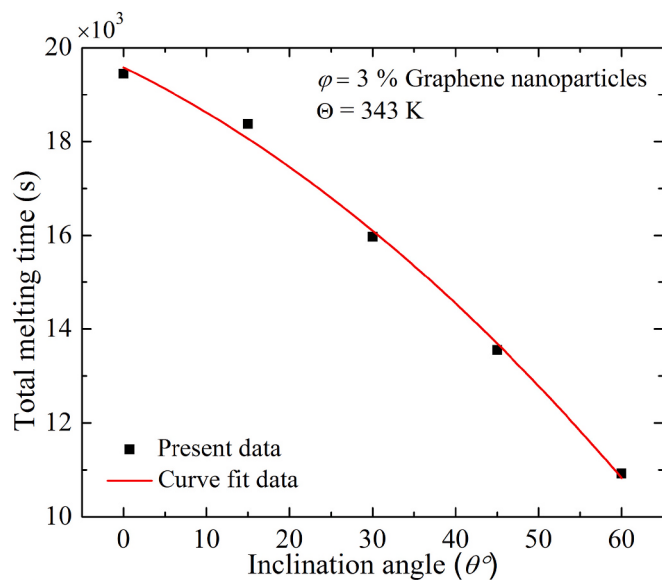


Fig. 20. Correlation between inclination angle (θ) and total melting time of Graphene-based NePCM at $\Theta = 343$ K.

buoyancy-driven currents, resulting in improved melting rates up to 44.865 % for NePCM compared to a horizontal configuration. The type and concentration of nanoparticles also influence performance, with Graphene nanoparticles outperforming Al_2O_3 and CuO , especially at lower concentrations. However, beyond 1 % concentration, the benefits taper off as higher viscosity and reduced latent heat limit further gains. These findings highlight the importance of optimizing nanoparticle selection, concentration, and system geometry to maximize the efficiency of NePCMs in thermal energy storage applications.

Furthermore, an analytical approach has been utilized to develop a mathematical correlation between inclination angle (θ) and total melting time, which is shown in Fig. 20. In this analysis, the Graphene nanoparticles (with $\varphi = 3\%$) mixed NePCM at $\Theta = 343\text{ K}$ are taken into consideration as a best parametric conditions. The data indicates that the total melting time lowers as the inclination angle increases. A polynomial curve fitting (quadratic equation) is used to model the trend:

$$y = A + B_1x + B_2x^2 \quad (19)$$

where x represents the inclination angle (θ°). The fitted curve demonstrates a strong correlation, with an adjusted R^2 value of 0.99343, indicating an excellent fit between the model and the data. The parameters from the optimization study are:

$A: 19579.48571$ (with a standard error of 266.25668)

$B_1: -86.0181$ (with a standard error of 21.02679)

$B_2: -0.99714$ (with a standard error of 0.33605)

The above correlation study reveals that as the inclination angle increases from $\theta = 0^\circ$ to 60° , the total melting time decreases significantly, indicating that higher angles promote faster melting. This curve fitting is done by polynomial curve fitting. This relationship follows a quadratic trend, where the rate of reduction in melting time slows down at higher angles, as depicted by the concave curve. The fitted model suggests that increasing the inclination angle improves melting efficiency. Thus, the study highlights that optimizing the inclination angle is crucial for minimizing melting time, with higher angles facilitating faster heat transfer, although the rate of improvement decreases beyond certain values.

From the analysis optimal design conditions are recommended for a similar thermal system. So, this research identifies the best geometric layouts and flow control factors. It is observed that the best energy efficiency is achieved for a volume fraction of Graphene nanoparticles $\varphi = 3\%$, a geometry inclination angle of $\theta = 60^\circ$, and a wall temperature of $\Theta = 343\text{ K}$ and it optimized the thermal energy storage capacity and melting performance.

5. Conclusions

This study aims to numerically explore the improved heat transfer capabilities of PCMs in an oriented rectangular cavity containing paraffin wax PCM (RT-45) mixed with various types and concentrations of nanoparticles. The volume of the PCM (3120 mm^3) remains consistent across all the scenarios. This study examines the impact of nanoparticle concentration (φ), nanoparticle type (Al_2O_3 , CuO , and Graphene), an inclination angle of the cavity (θ), and heated wall temperature variation (Θ). By pinpointing the optimal concentration, and correct type of nanoparticle and inclination angles, engineers and researchers can craft more effective PCM-based thermal energy storage setups for a range of uses, including solar energy capture, building climate control, and electronic thermal management. The major findings of this study are summarized below:

- Impact of nanoparticles and the volume fraction:** A 3 % volume fraction of nanoparticles is optimal for cost and thermal performance. Graphene nanoparticles outperforms CuO and Al_2O_3 due to its high conductivity and low density. At $\varphi = 0.5\%$ concentration,

Al_2O_3 shows the highest enhancement (4.975 %), but at $\varphi = 3\%$, Graphene nanoparticles leads with a 7.118 % enhancement.

- Impact of cavity inclination:** According to the study, the NePCM performance of the module is greatly impacted by the inclination angle of the cavity of a thermal energy storage system. As the angle θ increases from 0° to 15° , 30° , 45° , and 60° , the melting rate of pure PCM improves by 5.492 %, 17.860 %, 30.316 %, and 43.841 %, respectively. For NePCM, the enhancements are 8.053 %, 19.778 %, 31.787 %, and 44.865 % compared to pure PCM at $\theta = 0^\circ$.
- Impact of heated wall temperature variation:** it is concluded that the PCM undergoes a phase change when the wall temperature is above $\Theta = 322\text{ K}$. At $\Theta = 323\text{ K}$, the PCM starts melting, and higher wall temperatures of $\Theta = 333\text{ K}$ and 343 K accelerate the melting process double and triple respectively, enhancing heat transfer within the cavity.
- Optimal energy storage capacity:** The investigation shows that adding 0.5 % Al_2O_3 nanoparticles boosts NePCM-based thermal storage systems, achieving an energy storage rate of 1223.687 J/min, outperforming CuO but not Graphene nanoparticles. Graphene nanoparticles, with rates ranging from 1232.602 to 1299.191 J/min, consistently performs best. Higher inclination angles, especially $\theta = 60^\circ$, double the energy storage rate compared to $\theta = 0^\circ$, highlighting Graphene-based PCM composites' efficiency in thermal storage.
- Enhanced melting rate:** Increasing nanoparticle volume in NePCM accelerates melting and boosts energy efficiency. Adding 0.5 % Al_2O_3 nanoparticles enhances thermal performance with a melting speed of 8.759 g/min, higher than Graphene (8.587 g/min) and CuO (8.556 g/min) nanoparticles. At $\varphi = 1\%$, the speed decreases slightly to 8.648 g/min. Graphene is most effective at $\varphi = 1\%-5\%$ volume fraction, with speeds ranging from 8.823 to 9.299 g/min. NePCM consistently outperforms pure PCM, with melting speeds doubling at a 60° angle.
- Trade-offs in material properties:** The study shows that adding nanoparticles to NePCM improves thermal conductivity and density but reduces specific heat. Higher nanoparticle volume fractions increase viscosity, complicating the melting process, the gains in conductivity, and the reduction in latent heat.
- Geometry and Flow Control:** The study concluded that for the best energy efficiency, $\varphi = 3\%$ volume fraction of Graphene nanoparticles, an inclination angle of $\theta = 60^\circ$, and a wall temperature of $\Theta = 343\text{ K}$ optimized the thermal energy storage capacity and melting performance.

This study emphasizes the critical role of environmental conditions and system design—particularly the tilt angle—in optimizing the thermal energy storage performance of NePCMs. For systems such as photovoltaic panels that use PCMs for passive cooling, tilt angle significantly affects heat transfer. NePCMs hold promise for renewable energy applications like solar thermal storage, waste heat recovery, and thermal regulation. Further research is necessary to investigate additional factors impacting system efficiency and to enable the practical deployment of NePCM technology in real-world scenarios.

Nonetheless, this study has some limitations. It only examines three nanoparticles (Al_2O_3 , CuO , and Graphene), excluding other potential nanomaterials. Exploring alternatives like silicon carbide (SiC) or zinc oxide (ZnO) could reveal more effective or economical options. Additionally, the study relies on CFD simulations, which may not fully represent the complexities of real-world conditions. Future research should focus on conducting real-world experiments to validate the findings and overcome these limitations, ensuring a broader understanding of NePCMs for various energy storage applications.

Future perspective:

Future research should focus on expanding the current findings by incorporating three-dimensional effects to capture the full complexity of NePCM behavior. Additionally, experiments under diverse boundary conditions, including variations in temperature, pressure, and

environmental factors, should be conducted. It is also essential to validate the theoretical advancements through real-world applications, connecting the lab-based results with practical energy storage systems for cleaner energy solutions in industries like solar power and thermal management.

CRediT authorship contribution statement

Anjan Nandi: Writing – original draft, Validation, Supervision, Software, Resources, Methodology, Investigation, Formal analysis, Data curation. **Nirmalendu Biswas:** Writing – review & editing, Visualization, Validation, Supervision, Resources, Formal analysis, Conceptualization.

Declaration of competing interest

The authors declare that they have no known competing financial interests or personal relationships that could have appeared to influence the work reported in this paper.

Acknowledgments

This work has been supported by the AICTE doctoral fellowship program (under ADF 2022-2023), SERB-SRG project fund (Grant No. SRG/2021/001388) of the Government of India, and WBDST project fund (Grant No.: STBT-11012(16)/2/2023-ST SEC), respectively.

Data availability

The article contains all the data supporting the study's findings.

References

- [1] I. Dincer, M.A. Rosen, *Thermal Energy Storage (TES). Thermal Energy Storage: Systems and Applications*, John Wiley & Sons Ltd., England, 2002.
- [2] S.L. Tariq, H.M. Ali, M.A. Akram, M.M. Janjua, M. Ahmadlouydarab, Nanoparticles enhanced phase change materials (NePCMs)-a recent review, *Appl. Therm. Eng.* 176 (2020) 115305.
- [3] A. Sharma, V.V. Tyagi, C.R. Chen, D. Buddhi, Review on thermal energy storage with phase change materials and applications, *Renew. Sust. Energ. Rev.* 13 (2) (2009) 318–345.
- [4] H. Rieger, U. Projahn, M. Bareiss, H. Beer, Heat transfer during melting inside a horizontal tube, *J. Heat Transf.* 105 (2) (1983) 226–234.
- [5] B. Kamkari, D. Groulx, Experimental investigation of melting behaviour of phase change material in finned rectangular enclosures under different inclination angles, *Exp. Thermal Fluid Sci.* 97 (2018) 94–108.
- [6] M.E. Nakhchi, J.A. Esfahani, Improving the melting performance of PCM thermal energy storage with novel stepped fins, *Journal of Energy Storage* 30 (2020) 101424.
- [7] A. Nandi, N. Biswas, A. Datta, Enhanced melting behavior of phase change material (PCM) in a rectangular cavity: effect of fin, in: Conference on Fluid Mechanics and Fluid Power, Springer Nature Singapore, Singapore, 2022, pp. 277–288. December.
- [8] C.W. Robak, T.L. Bergman, A. Faghri, Enhancement of latent heat energy storage using embedded heat pipes, *Int. J. Heat Mass Transf.* 54 (15–16) (2011) 3476–3484.
- [9] H. Senobar, M. Aramesh, B. Shabani, Nanoparticles and metal foams for heat transfer enhancement of phase change materials: a comparative experimental study, *Journal of Energy Storage* 32 (2020) 101911.
- [10] H.E. Abdelrahman, M.H. Wahba, H.A. Refaei, M. Moawad, N.S. Berbish, Performance enhancement of photovoltaic cells by changing configuration and using PCM (RT35HC) with nanoparticles Al_2O_3 , *Sol. Energy* 177 (2019) 665–671.
- [11] C.J. Ho, J.Y. Gao, An experimental study on melting heat transfer of paraffin dispersed with Al_2O_3 nanoparticles in a vertical enclosure, *Int. J. Heat Mass Transf.* 62 (2013) 2–8.
- [12] M. Jourabian, M. Farhadi, A.A.R. Darzi, Outward melting of ice enhanced by Cu nanoparticles inside cylindrical horizontal annulus: lattice Boltzmann approach, *Appl. Math. Model.* 37 (20–21) (2013) 8813–8825.
- [13] S. Sharma, L. Micheli, W. Chang, A.A. Tahir, K.S. Reddy, T.K. Mallick, Nano-enhanced phase change material for thermal management of BICPV, *Appl. Energy* 208 (2017) 719–733.
- [14] S. Jesumathy, M. Udayakumar, S. Suresh, Experimental study of enhanced heat transfer by addition of CuO nanoparticle, *Heat Mass Transf.* 48 (2012) 965–978.
- [15] D. Zou, X. Ma, X. Liu, P. Zheng, Y. Hu, Thermal performance enhancement of composite phase change materials (PCM) using graphene and carbon nanotubes as additives for the potential application in lithium-ion power battery, *Int. J. Heat Mass Transf.* 120 (2018) 33–41.
- [16] Z. Khan, Z.A. Khan, Role of extended fins and graphene nano-platelets in coupled thermal enhancement of latent heat storage system, *Energy Convers. Manag.* 224 (2020) 113349.
- [17] M.R. Safaei, H.R. Goshayeshi, I. Chaer, Solar still efficiency enhancement by using graphene oxide/paraffin nano-PCM, *Energies* 12 (10) (2019) 2002.
- [18] L. Xu, Y. Zhang, J. Li, L. Zhang, Z. Yuan, H.S. Majdi, M. Hekmatifar, Thermal behavior and phase transition of the aminostaldehyde as the wall and bromohexadecane as a phase change material enriched via gold nanoparticles: Molecular dynamics study, *Journal of Energy Storage* 55 (2022) 105482.
- [19] N. Pradeep, K. Paramasivam, T. Rajesh, V.S. Purusothamanan, S. Iyahraja, Silver nanoparticles for enhanced thermal energy storage of phase change materials, *Materials Today: Proceedings* 45 (2021) 607–611.
- [20] J.L. Zeng, L.X. Sun, F. Xu, Z.C. Tan, Z.H. Zhang, J. Zhang, T. Zhang, Study of a PCM based energy storage system containing Ag nanoparticles, *J. Therm. Anal. Calorim.* 87 (2007) 371–375.
- [21] H. Maher, K.A. Rocky, R. Bassiouny, B.B. Saha, Synthesis and thermal characterization of paraffin-based nanocomposites for thermal energy storage applications, *Thermal Science and Engineering Progress* 22 (2021) 100797.
- [22] A.H. Al-Waeli, M.T. Chaichan, H.A. Kazem, K. Sopian, Comparative study to use nano-(Al_2O_3 , CuO , and SiC) with water to enhance photovoltaic thermal PV/T collectors, *Energy Convers. Manag.* 148 (2017) 963–973.
- [23] A. Babapoor, A.R. Haghghi, S.M. Jokar, M. Ahmadi Mezjin, The performance enhancement of paraffin as a PCM during the solidification process: utilization of graphene and metal oxide nanoparticles, *Iran. J. Chem. Chem. Eng.* 41 (1) (2022) 37–48.
- [24] H.S. Bae, M.K. Lee, W.W. Kim, C.K. Rhee, Dispersion properties of TiO_2 nanopowder synthesized by homogeneous precipitation process at low temperatures, *Colloids and surfaces A* 220 (1–3) (2003) 169–177.
- [25] S. Harikrishnan, M. Deenadhayan, S. Kalaiselvam, Experimental investigation of solidification and melting characteristics of composite PCMs for building heating application, *Energy Convers. Manag.* 86 (2014) 864–872.
- [26] T.P. Teng, C.C. Yu, Characteristics of phase-change materials containing oxide nano-additives for thermal storage, *Nanoscale Res. Lett.* 7 (2012) 1–10.
- [27] J. Wang, H. Xie, Z. Xin, Y. Li, L. Chen, Enhancing thermal conductivity of palmitic acid based phase change materials with carbon nanotubes as fillers, *Sol. Energy* 84 (2) (2010) 339–344.
- [28] F. Bahiraei, A. Fartaj, G.A. Nazri, Experimental and numerical investigation on the performance of carbon-based nanoenhanced phase change materials for thermal management applications, *Energy Convers. Manag.* 153 (2017) 115–128.
- [29] A. Zabalegui, D. Lokapur, H. Lee, Nanofluid PCMs for thermal energy storage: latent heat reduction mechanisms and a numerical study of effective thermal storage performance, *Int. J. Heat Mass Transf.* 78 (2014) 1145–1154.
- [30] A.R. Abdulmunem, P.M. Samin, H.A. Rahman, H.A. Hussien, I.I. Mazali, H. Ghazali, Experimental and numerical investigations on the effects of different tilt angles on the phase change material melting process in a rectangular container, *Journal of Energy Storage* 32 (2020) 101914.
- [31] Y. Wang, J. Dai, D. An, Numerical investigations on melting behavior of phase change material in a rectangular cavity at different inclination angles, *Appl. Sci.* 8 (9) (2018) 1627.
- [32] S. Xie, W. Wu, Effect of aspect ratio on PCM melting behavior in a square cavity, *International Communications in Heat and Mass Transfer* 143 (2023) 106708.
- [33] M.H. Hekmat, M.H.K. Haghani, E. Izadpanah, H. Sadeghi, The influence of energy storage container geometry on the melting and solidification of PCM, *International Communications in Heat and Mass Transfer* 137 (2022) 106237.
- [34] B. Kamkari, H.J. Amlashi, Numerical simulation and experimental verification of constrained melting of phase change material in inclined rectangular enclosures, *International Communications in Heat and Mass Transfer* 88 (2017) 211–219.
- [35] L. Colla, D. Ercole, L. Fedele, S. Mancin, O. Manca, S. Bobbo, Nano-phase change materials for electronics cooling applications, *J. Heat Transf.* 139 (5) (2017) 052406.
- [36] H.F. Öztürk, B. Kiyak, N. Biswas, F. Selimefendigil, H. Coşanay, Analysis of solidification of phase change material flowing through a channel with backward step: effects of step curvature, *Thermal Science and Engineering Progress* 9 (2024) 102439.
- [37] H.S. Sultan, H.I. Mohammed, N. Biswas, H. Togun, R.K. Ibrahim, J.M. Mahdi, W. Yaici, A. Keshmiri, P. Talebizadehsardari, Revolutionizing latent heat storage: boosting discharge performance with innovative undulated PCM container shapes in vertical shell-and-tube systems, *Journal of Computational Design and Engineering* 11 (2) (2024) 122–145.
- [38] H.F. Öztürk, H. Coşanay, N. Biswas, F. Selimefendigil, Thermal energy storage via waste heat from finned heater by using different phase change materials in a closed space, *Journal of Energy Storage* 70 (2023) 108002.
- [39] B. Kamkari, H. Shokouhmand, Experimental investigation of phase change material melting in rectangular enclosures with horizontal partial fins, *Int. J. Heat Mass Transf.* 78 (2014) 839–851.
- [40] N.B. Khedher, N. Biswas, H. Togun, H.I. Mohammed, J.M. Mahdi, R.K. Ibrahim, P. Talebizadehsardari, Geometry modification of a vertical shell-and-tube latent heat thermal energy storage system using a framed structure with different undulated shapes for the phase change material container during the melting process, *Journal of Energy Storage* 72 (2023) 108365.
- [41] H. Togun, H.S. Sultan, H.I. Mohammed, A.M. Sadeq, N. Biswas, H.A. Hasan, R. Z. Homod, A.H. Abdulkadhim, Z.M. Yaseen, P. Talebizadehsardari, A critical review on phase change materials (PCM) based heat exchanger: different hybrid techniques for the enhancement, *Journal of Energy Storage* 79 (2024) 109840.

- [42] A.D. Brent, V.R. Voller, K.T.J. Reid, Enthalpy-porosity technique for modeling convection-diffusion phase change: application to the melting of a pure metal, *Numerical Heat Transfer, Part A* 13 (3) (1988) 297–318.
- [43] N. Biswas, D. Chatterjee, S. Sarkar, N.K. Manna, Magneto-nanofluidic thermal transport and irreversibility in semicircular systems with heated wavy bottom under constant fluid volume and cooling surface constraints, *International Journal of Numerical Methods for Heat & Fluid Flow* 34 (2) (2024) 1021–1059.
- [44] H.F. Öztop, H. Coşanay, N. Biswas, F. Selimefendigil, Analysis of natural convection and melting in a separated cavity with nano-enhanced phase change material filled wall, *Arab. J. Sci. Eng.* 49 (2024) 10653–10668.
- [45] N.K. Manna, A. Saha, N. Biswas, K. Ghosh, Shape matters: convection and entropy generation in magneto-hydrodynamic nanofluid flow in constraint-based analogous annular thermal systems, *Numerical Heat Transfer, Part A* (2024) 1–33, <https://doi.org/10.1080/10407782.2024.2347585>.
- [46] H.F. Öztop, H. Coşanay, N. Biswas, F. Selimefendigil, N. Abu-Hamdeh, Melting behavior of layered different phase change materials for a cylinder insert into a channel, *Thermal Science and Engineering Progress* 51 (2024) 102638.
- [47] J.M. Khodadadi, S.F. HosseiniZadeh, Nanoparticle-enhanced phase change materials (NEPCM) with great potential for improved thermal energy storage, *International Communications in Heat and Mass Transfer* 34 (5) (2007) 534–543.
- [48] N. Wakao, S. Kagei, *Heat and Mass Transfer in Packed Beds Vol. 1*, Taylor & Francis, 1982.
- [49] H.C. Brinkman, The viscosity of concentrated suspensions and solutions, *J. Chem. Phys.* 20 (4) (1952) 571.
- [50] M.A. Said, H. Togun, A.M. Abed, N. Biswas, H.I. Mohammed, H.S. Sultan, J. M. Mahdi, P. Talebizadehsardari, Evaluation of wavy wall configurations for accelerated heat recovery in triplex-tube energy storage units for building heating applications, *Journal of Building Engineering* 94 (2024) 109762.
- [51] H.F. Öztop, B. Kiyak, N. Biswas, F. Selimefendigil, H. Coşanay, Effects of cooler shape and position on solidification of phase change material in a cavity, *J. Taiwan Inst. Chem. Eng.* 163 (2024) 105628.
- [52] J.M. Mahdi, H.M.T. Al-Najjar, H. Togun, N. Biswas, M. Boujelbene, S. Alshammari, P. Talebizadehsardari, Year-round performance evaluation of photovoltaic-thermal collector with nano-modified phase-change material for building application in an arid desert climate zone, *Energy and Buildings* 320 (2024) 114597.
- [53] B. Kiyak, H.F. Oztop, N. Biswas, F. Selimefendigil, Effects of geometrical configurations on melting and solidification processes in phase change materials, *Appl. Therm. Eng.* 258 (2025) 124726.
- [54] N.B. Khedher, H.I. Mohammed, A.M. Abed, N. Biswas, H. Togun, K.A. Hammoodi, J.M. Mahdi, P. Talebizadehsardari, Maximizing charging/discharging capabilities of horizontal shell-and-tube latent heat storage systems with innovative curved fin inserts, *Int. J. Heat Mass Transf.* 236 (2025) 126289.
- [55] T. Abdulrazzaq, N. Biswas, T. Alsharifi, F.L. Rashid, A.F. Khalaf, A.M. Sadeq, A. E. Anqi, H. Togun, A.K. Hussein, Performance improvement of phase change material (PCM)-based shell-and-tube-type latent heat energy storage system utilizing curved fins, *J. Therm. Anal. Calorim.* 149 (2024) 14241–14255.
- [56] ANSYS Fluent, Ansys Fluent Theory Guide 15317, Ansys Inc., USA, 2011, pp. 724–746.